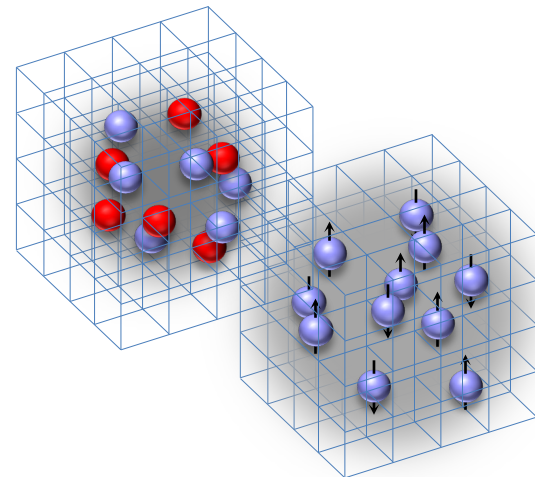


Nuclear Lattice Simulations

Lecture 2: Effective Field Theory and Nuclear Forces

Dean Lee (leed@frib.msu.edu)
Facility for Rare Isotope Beams
Michigan State University
Nuclear Lattice EFT Collaboration
June 24, 2020



ACPTP Nuclear Physics School 2020
June 22-26, 2020

Outline

Nuclear forces and effective theories

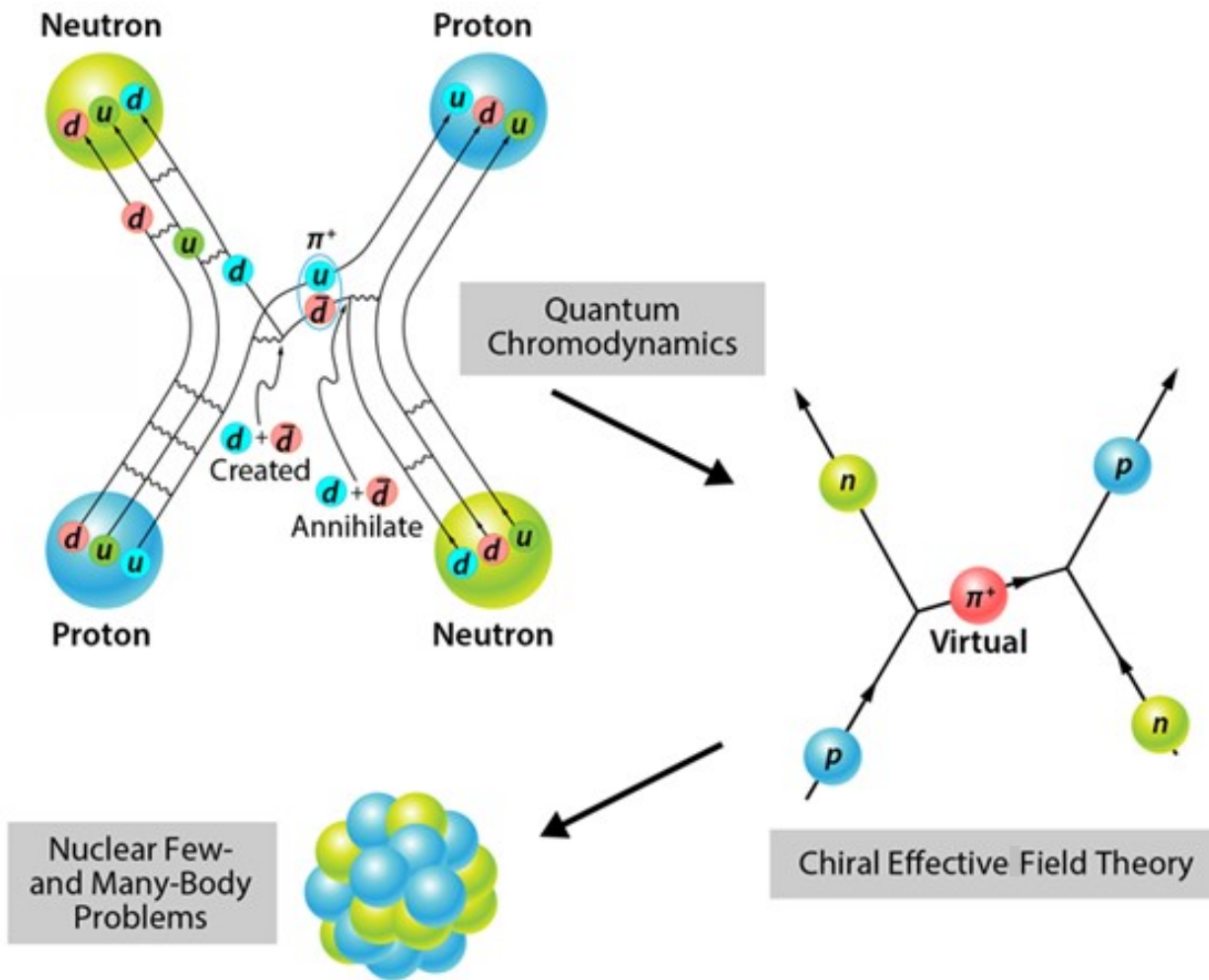
Chiral effective field theory

Spherical wall method

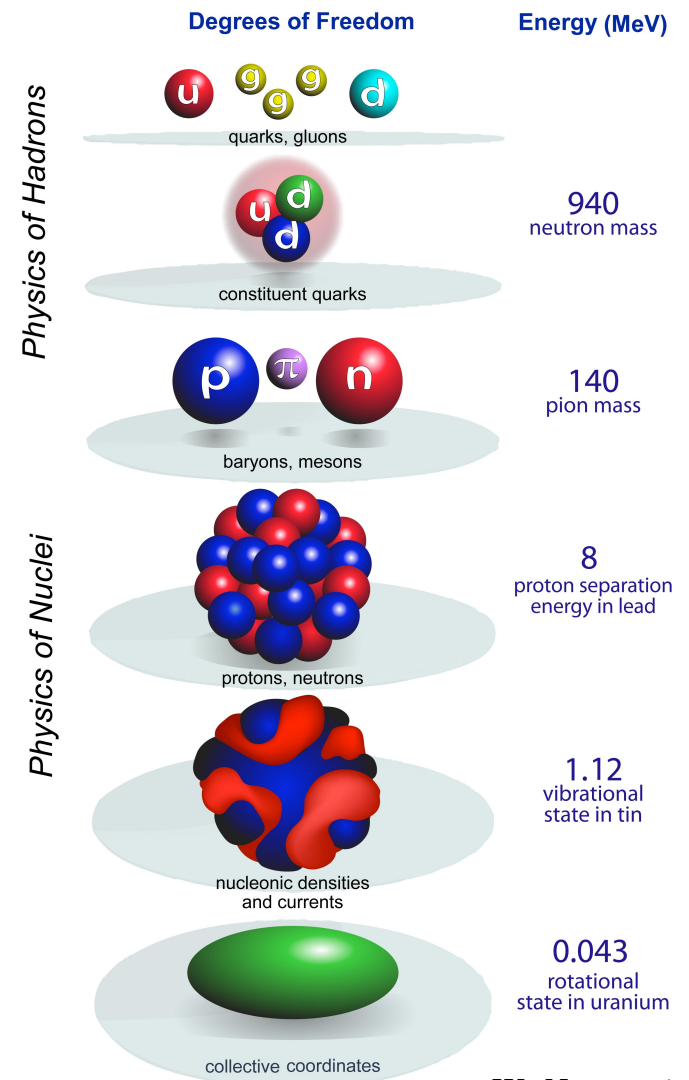
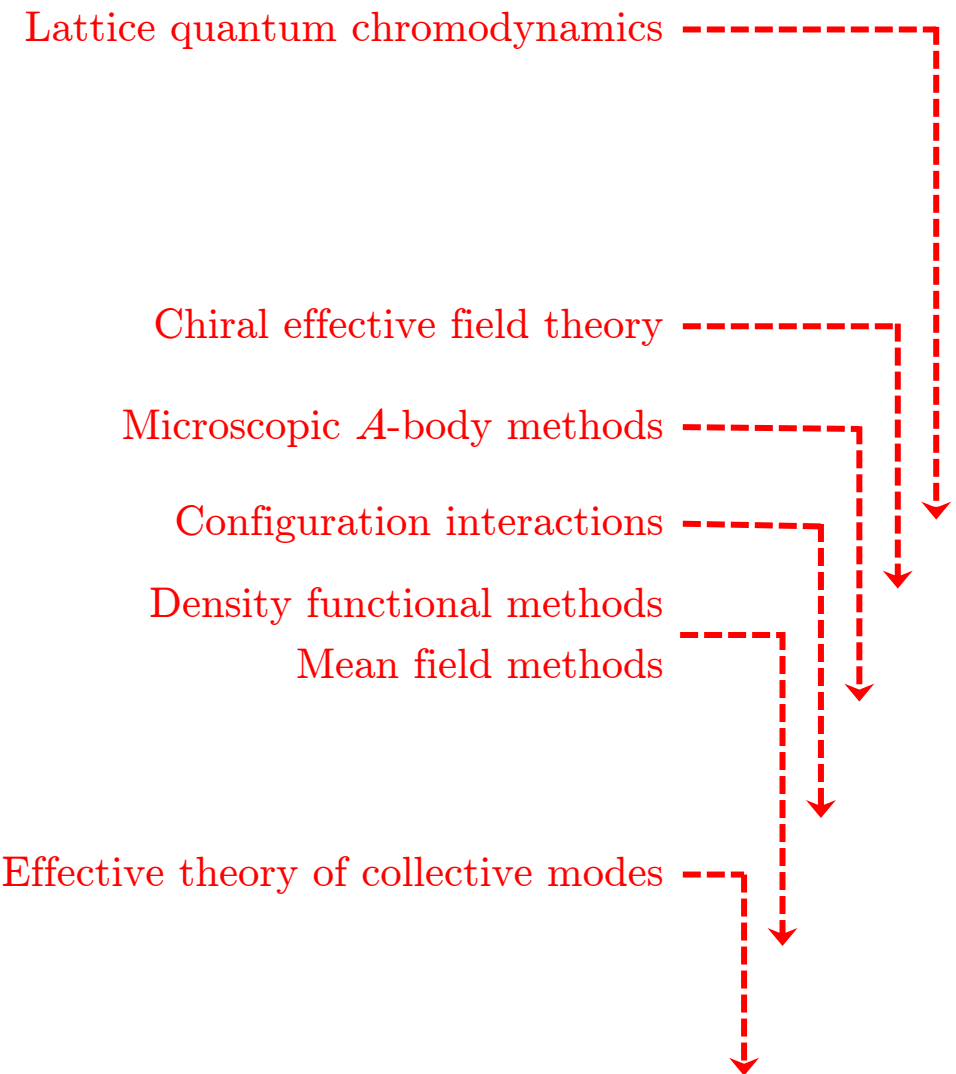
Chiral EFT interactions on the lattice

Eigenvector continuation

Nuclear forces



Effective field theories and energy scales

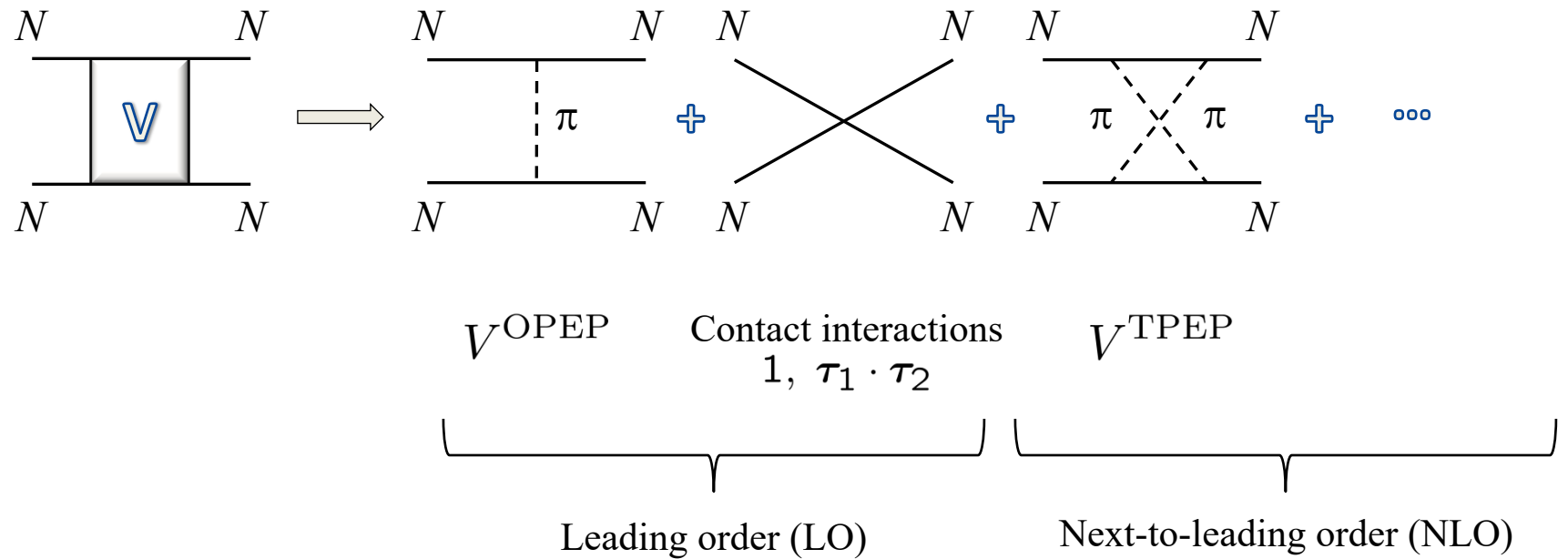


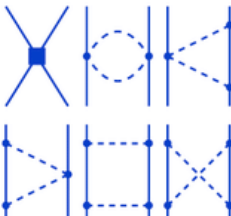
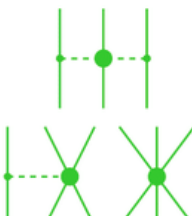
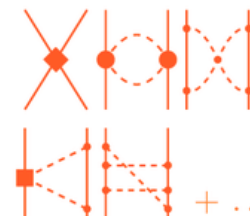
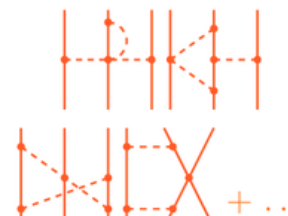
W. Nazarewicz

Chiral EFT for low-energy nucleons

Weinberg, PLB 251 (1990) 288; NPB 363 (1991) 3

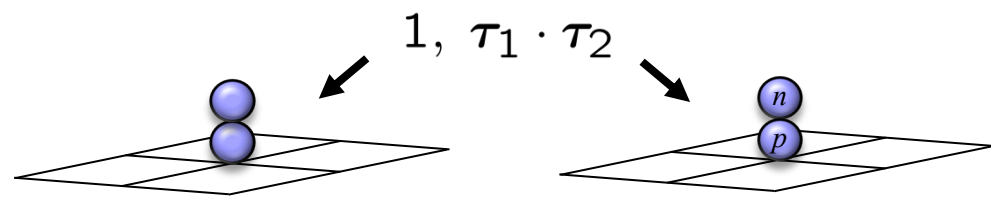
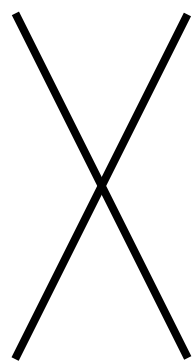
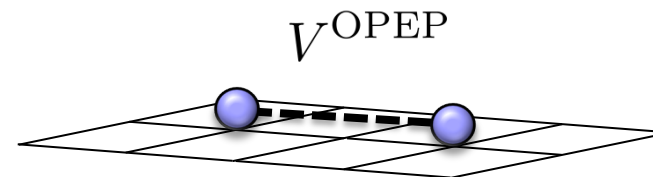
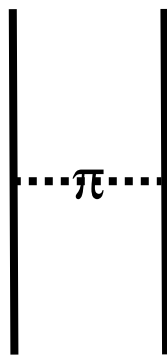
Construct the effective potential order by order



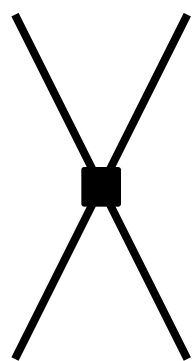
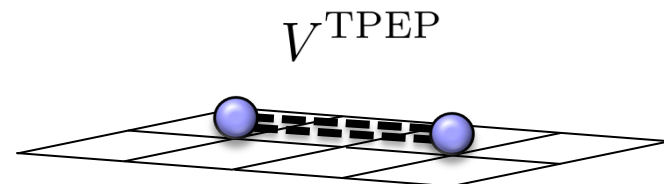
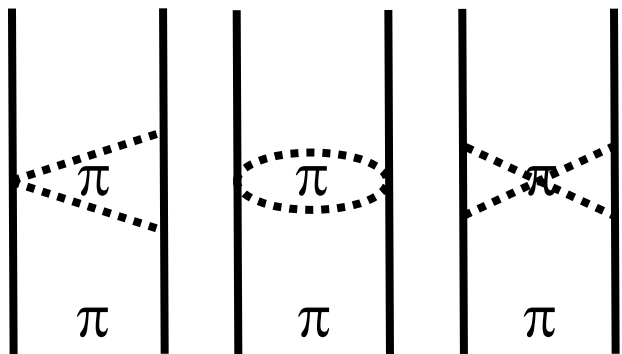
	NN	3N	4N
LO $(Q/\Lambda_\chi)^0$			
NLO $(Q/\Lambda_\chi)^2$			
NNLO $(Q/\Lambda_\chi)^3$			
N³LO $(Q/\Lambda_\chi)^4$			

Ordonez *et al.* 1994; Friar & Coon 1994; Kaiser *et al.* 1997; Epelbaum *et al.* 1998, 2003, ...;
Kaiser 1999-2001; Higa *et al.* 2003; ...

Leading order on the lattice



Next-to-leading order on the lattice

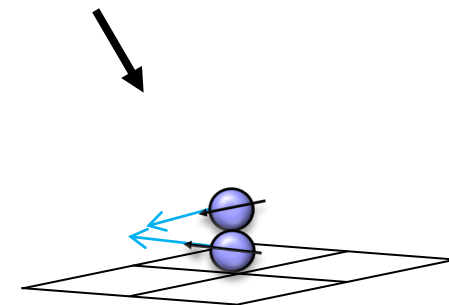
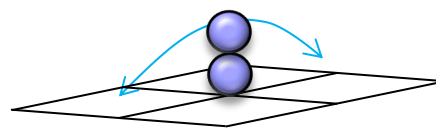


$$\vec{\nabla}_1 \cdot \vec{\nabla}_2$$

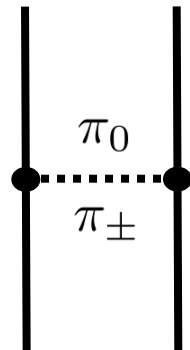


$$(\vec{\sigma}_1 \cdot \vec{\nabla}_1) (\vec{\sigma}_2 \cdot \vec{\nabla}_2)$$

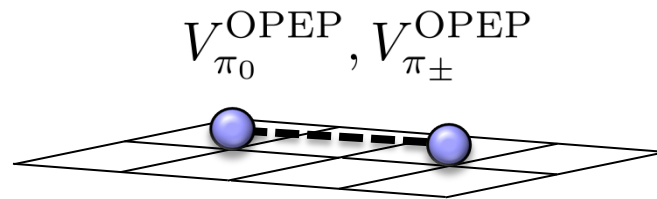
\cdots



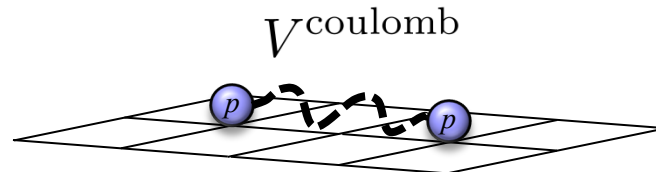
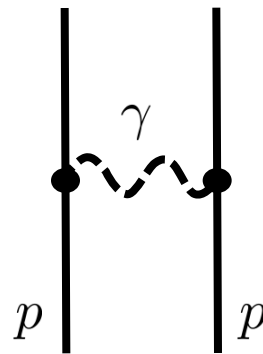
Pion mass difference



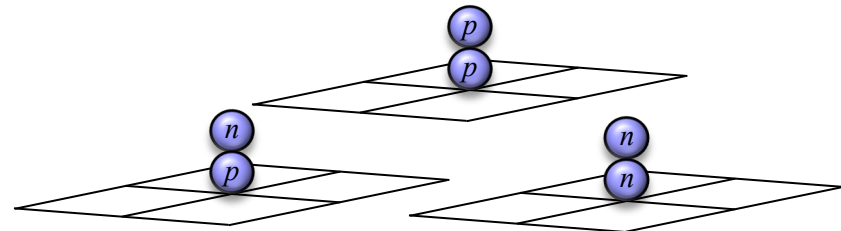
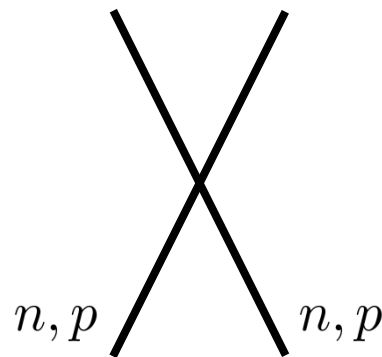
$$m_{\pi_0} \neq m_{\pi_\pm}$$



Coulomb potential

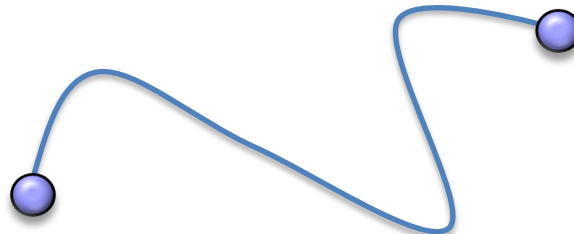


Charge symmetry breaking
Charge independence breaking



Spherical wall method

Imagine a massless string connecting two particles. There is no effect on the center-of-mass motion. However, the two particles cannot separate beyond the length of the string. We have imposed a hard spherical wall boundary condition on the relative motion.



This can now be used to extract scattering phase shifts for the two interacting particles.

Borasoy, Epelbaum, Krebs, D.L., Meißner, EPJA 34 (2007) 185

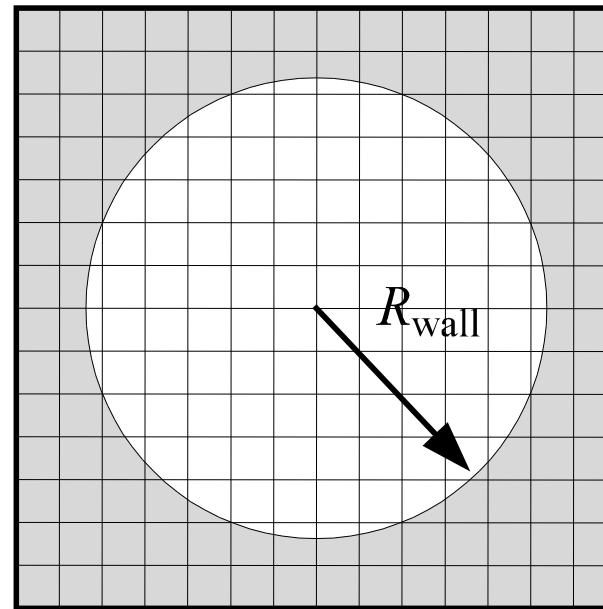
Lu, Lähde, D.L., Meißner, PLB 760 (2016) 309

Bovermann, Epelbaum, Krebs, D.L. arXiv:1905.02492

The spherical wall method has been used in continuous space calculations.

Carlson, Pandharipande, Wiringa, NPA 424 (1984) 47

But the method is particularly useful for finite-volume lattice calculations.



In particular, it removes the breaking of rotation symmetry caused by the periodic boundaries.

The radial Schrödinger equation gives

$$\left\{ -\frac{1}{2\mu} \frac{d}{dr} \left(r^2 \frac{d}{dr} \right) + \frac{\ell(\ell+1)}{2\mu r^2} + V(r) \right\} R(r) = ER(r)$$

$$u(r) = rR(r)$$

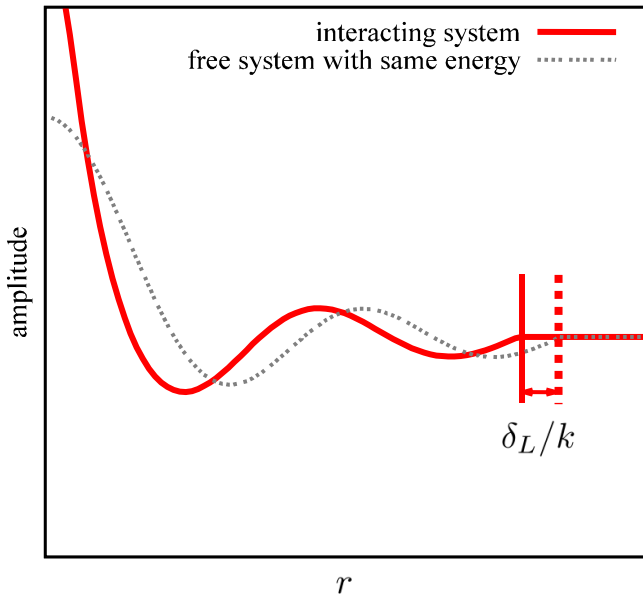
$$-\frac{1}{2\mu} \frac{d^2 u}{dr^2} + \left[\frac{\ell(\ell+1)}{2\mu r^2} + V(r) \right] u(r) = Eu(r)$$

Beyond the range of the interaction, the wave function has the form

$$R(r) \propto \cos \delta_\ell j_\ell(kr) - \sin \delta_\ell y_\ell(kr)$$

The wave function vanishes at the wall boundary. Therefore the phase shift is

$$\delta_\ell = \tan^{-1} \left[\frac{j_\ell(kR_{\text{wall}})}{y_\ell(kR_{\text{wall}})} \right]$$



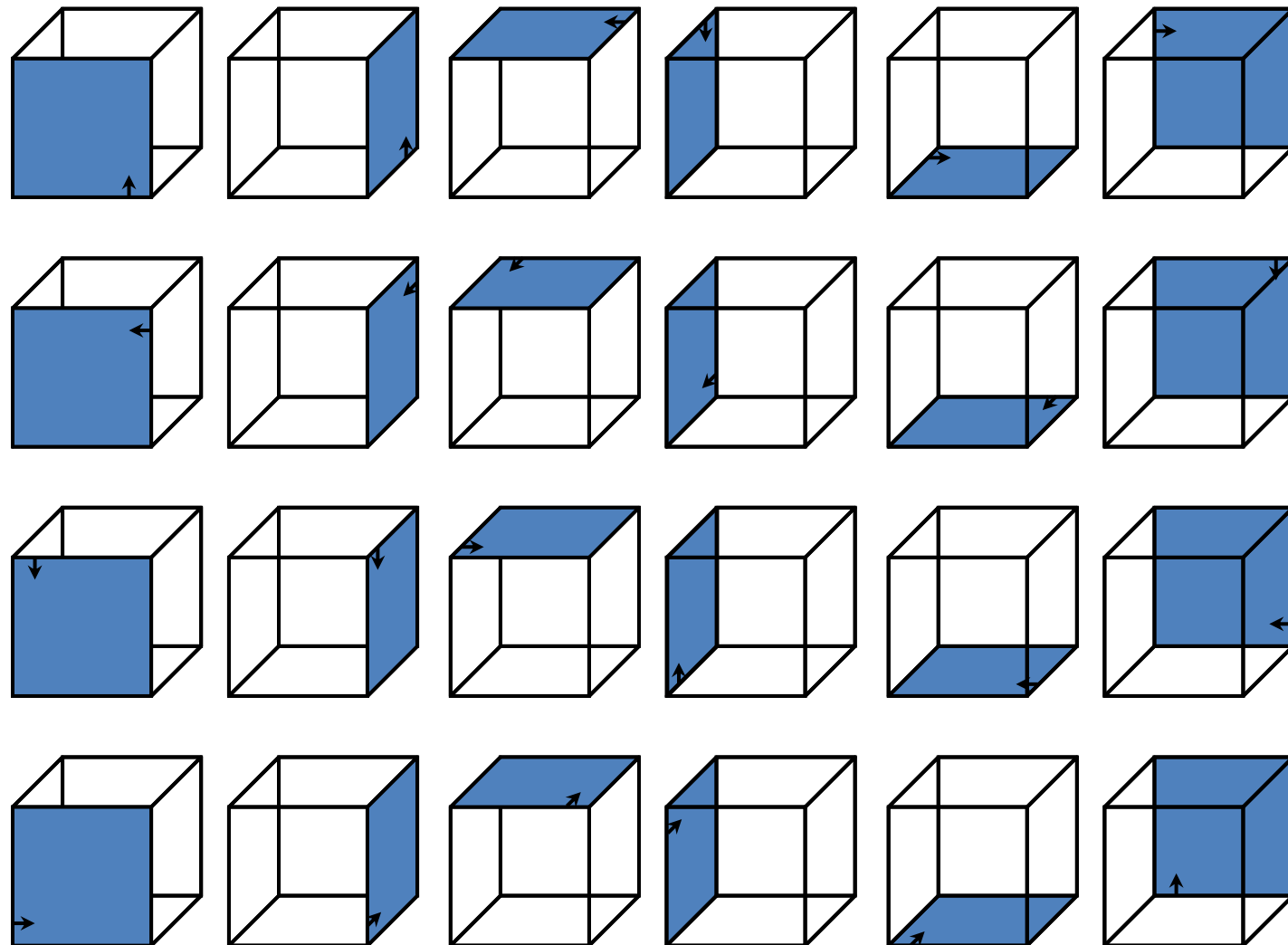
For the Coulomb case, the Bessel functions are replaced by Coulomb wave functions

$$\delta_\ell = \tan^{-1} \left[\frac{F_\ell(\eta, kR_{\text{wall}})}{G_\ell(\eta, kR_{\text{wall}})} \right]$$

where

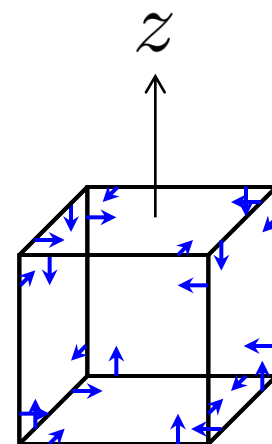
$$\eta = \frac{Z_1 Z_2 \alpha_{\text{EM}} m}{2k}$$

Cubic symmetry group



A_1

$$J_z = 0 \bmod 4$$

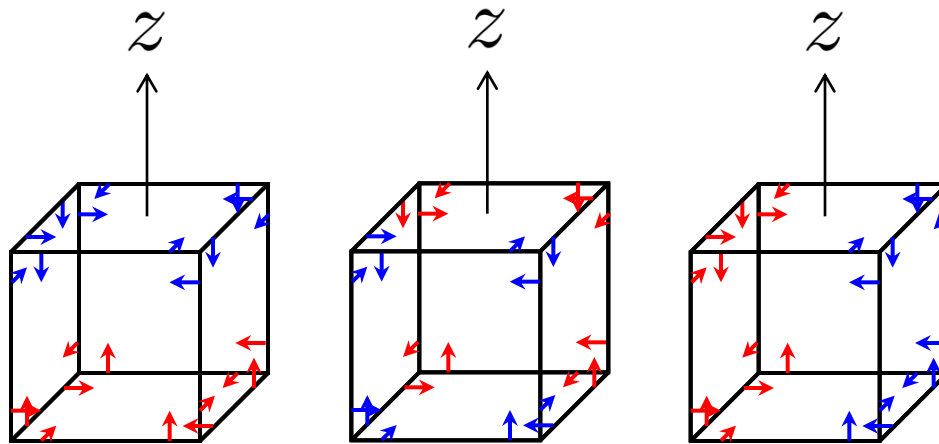


blue = +1

red = -1

T_1

$$J_z = 0, 1, 3 \bmod 4$$

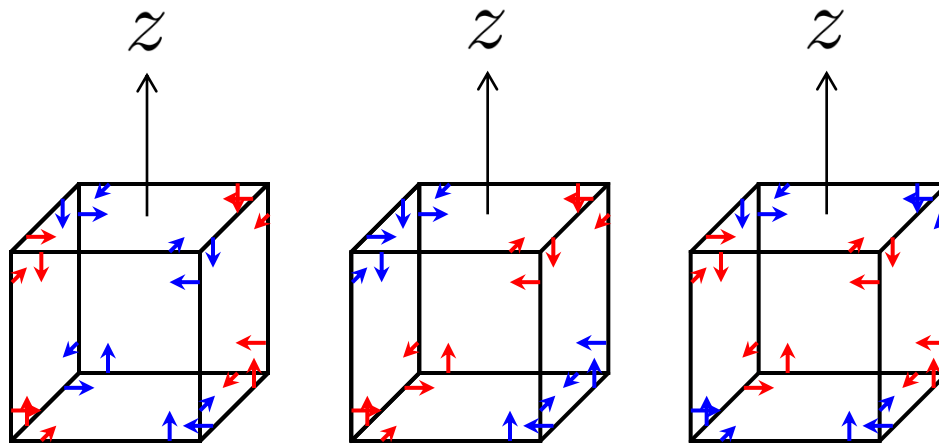


blue = +1

red = -1

T_2

$$J_z = 1, 2, 3 \bmod 4$$

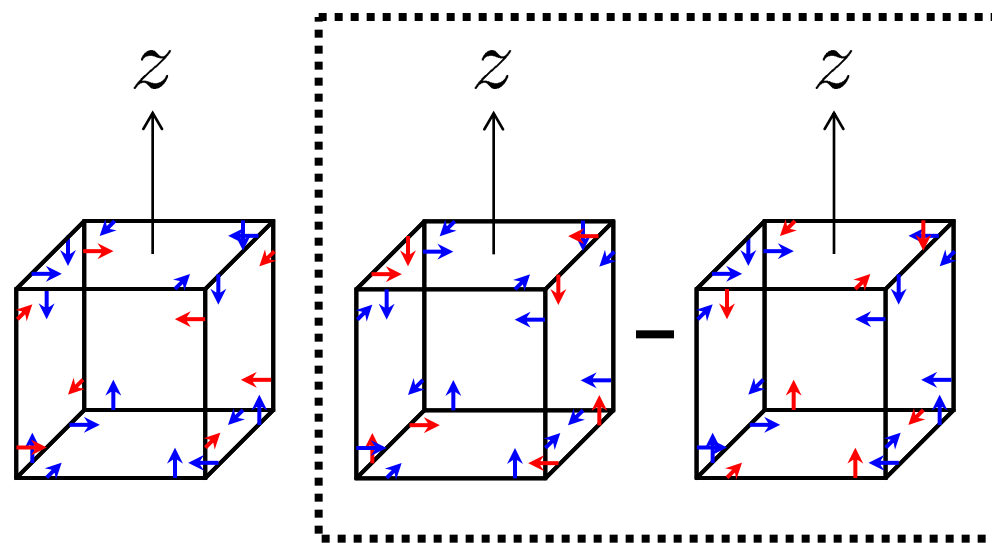


blue = +1

red = -1

E

$$J_z = 0, 2 \bmod 4$$

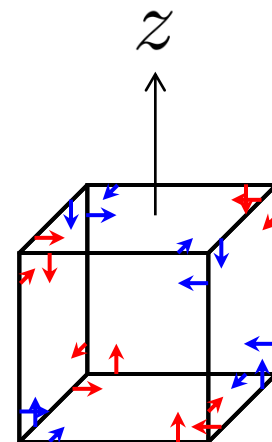


blue = +1

red = -2

A_2

$$J_z = 2 \bmod 4$$

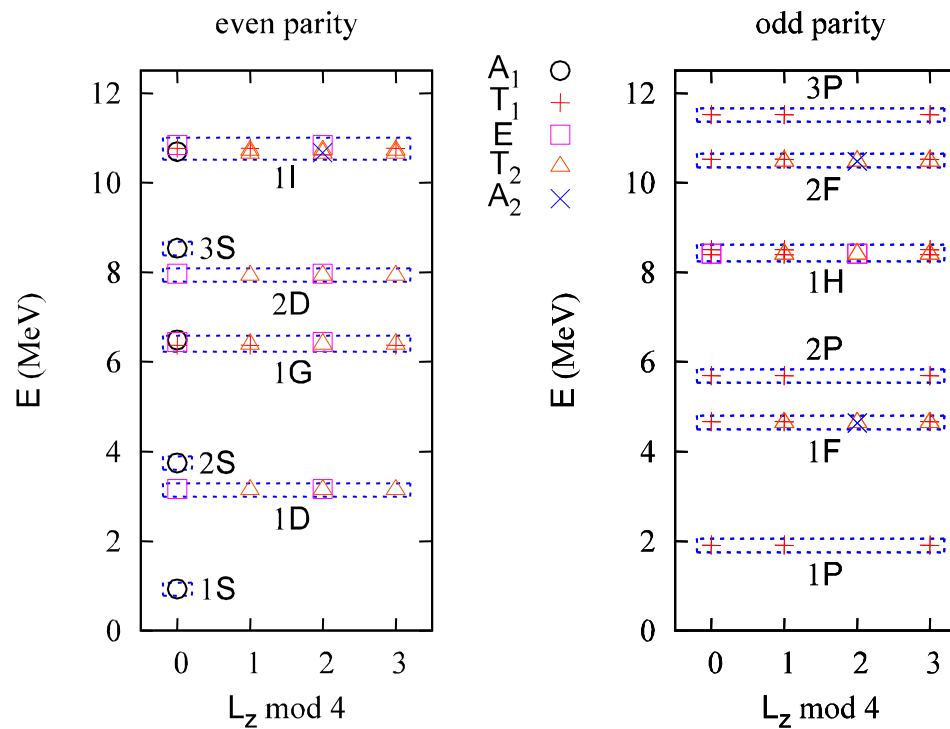


blue = +1

red = -1

Free energy levels

$$R_{\text{wall}} = 10a$$
$$a = 1.97 \text{ fm}$$



We can construct an approximate but surprisingly accurate radial equation by grouping together lattice coordinates with nearly the same magnitude and prescribing the angular dependence according to spherical harmonic projections

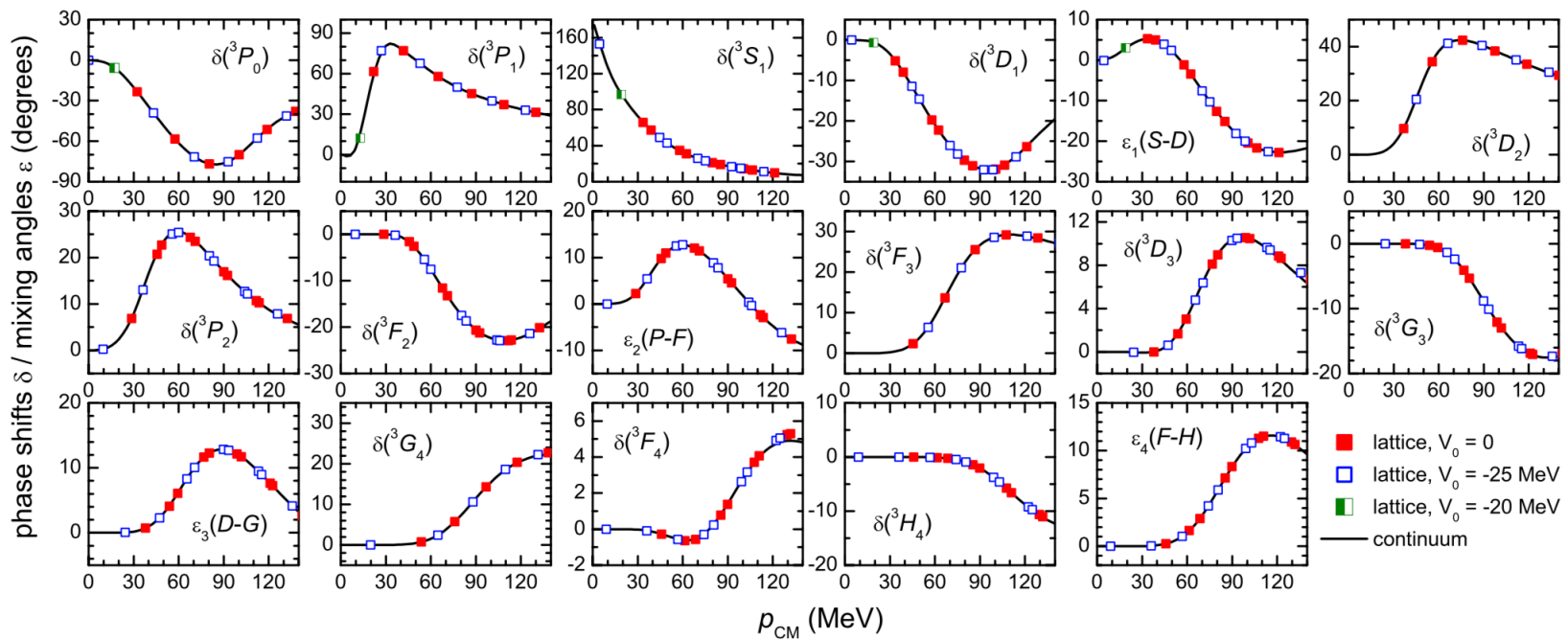
$$\psi(\vec{r}) = R(r_{\text{bin}})Y_{\ell,\ell_z}(\hat{r}), \quad ||\vec{r}| - r_{\text{bin}}| < \Delta_{\text{bin}}$$

For coupled channels in a finite volume, the mismatch of energy levels for the different channels is a nuisance. One can overcome this problem by interpolating the scattering data or fitting some functional form.

However in the spherical wall approach we can solve this problem for the case of two coupled channels by introducing a fictitious potential localized near the wall boundary that breaks time reversal invariance.

After breaking time reversal symmetry, the wave function and its complex conjugate are in general linearly independent. We can solve the coupled system for each energy level without interpolation or fitting.

Lu, Lähde, D.L., Meißner, PLB 760 (2016) 309



This has now been extended to an arbitrary number of coupled channels. The trick is that if we have N coupled channels, then we should make N identical copies of the system.

These copies are then coupled to each other through a fictitious potential that is localized near the spherical wall boundary.

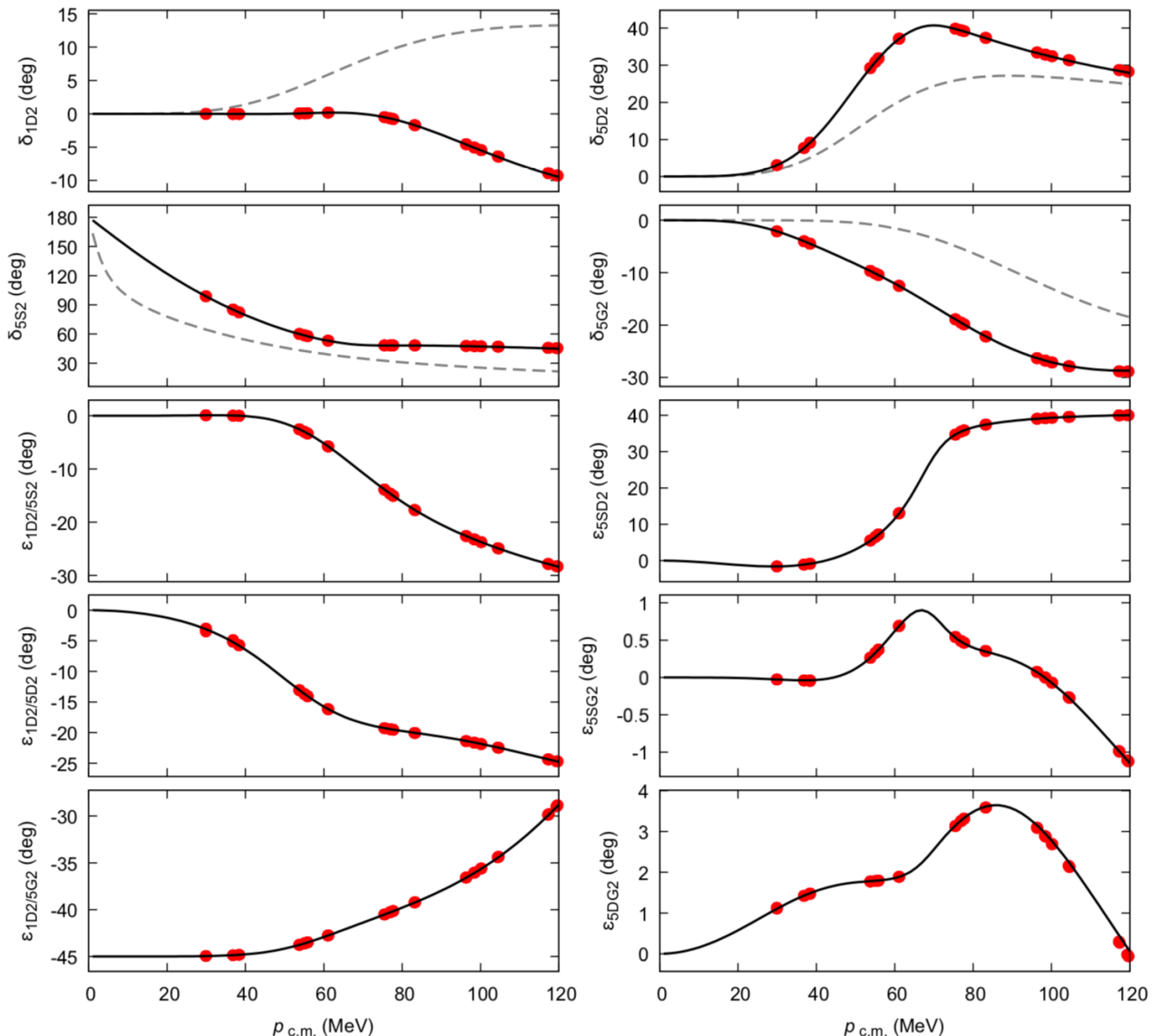


FIG. 8: (Color online.) Phase shifts and mixing angles for the $^1D_2/{}^5SDG_2$ -wave (black solid line: continuum; red points: lattice; gray dashed line: continuum results without channel mixing).

Chiral effective field theory on the lattice

We give an overview of chiral effective field theory interactions on the lattice. We define the smeared annihilation and creation operators.

$$a_{i,j}^{s_{\text{NL}}}(\mathbf{n}) = a_{i,j}(\mathbf{n}) + s_{\text{NL}} \sum_{|\mathbf{n}'|=1} a_{i,j}(\mathbf{n} + \mathbf{n}')$$

$$a_{i,j}^{s_{\text{NL}}\dagger}(\mathbf{n}) = a_{i,j}^\dagger(\mathbf{n}) + s_{\text{NL}} \sum_{|\mathbf{n}'|=1} a_{i,j}^\dagger(\mathbf{n} + \mathbf{n}')$$

Next we form bilinear functions of the annihilation operators with spin and isospin quantum numbers S, S_z, I, I_z .

$$[a(\mathbf{n})a(\mathbf{n}')]_{S,S_z,I,I_z}^{s_{\text{NL}}} = \sum_{i,j,i',j'} a_{i,j}^{s_{\text{NL}}}(\mathbf{n}) M_{ii'}(S, S_z) M_{jj'}(I, I_z) a_{i',j'}^{s_{\text{NL}}}(\mathbf{n}')$$

We introduce orbital angular momentum using solid spherical harmonics

$$R_{L,L_z}(\mathbf{r}) = \sqrt{\frac{4\pi}{2L+1}} r^L Y_{L,L_z}(\theta, \phi),$$

that are written as functions of the lattice derivatives on one of the annihilation operators

$$P_{S,S_z,L,L_z,I,I_z}^{2M,s_{NL}}(\mathbf{n}) = [a(\mathbf{n}) \nabla_{1/2}^{2M} R_{L,L_z}^*(\nabla) a(\mathbf{n})]_{S,S_z,I,I_z}^{s_{NL}}$$

We then project onto the selected spin and orbital angular momentum using Clebsch-Gordan coefficients

$$O_{S,L,J,J_z,I,I_z}^{2M,s_{NL}}(\mathbf{n}) = \sum_{S_z,L_z} \langle SS_z LL_z | JJ_z \rangle P_{S,S_z,L,L_z,I,I_z}^{2M,s_{NL}}(\mathbf{n})$$

We use these structures to construct the short-range interactions. We also specifically construct a short-range interaction that is Wigner SU(4) symmetric at leading-order with a tunable local regulator.

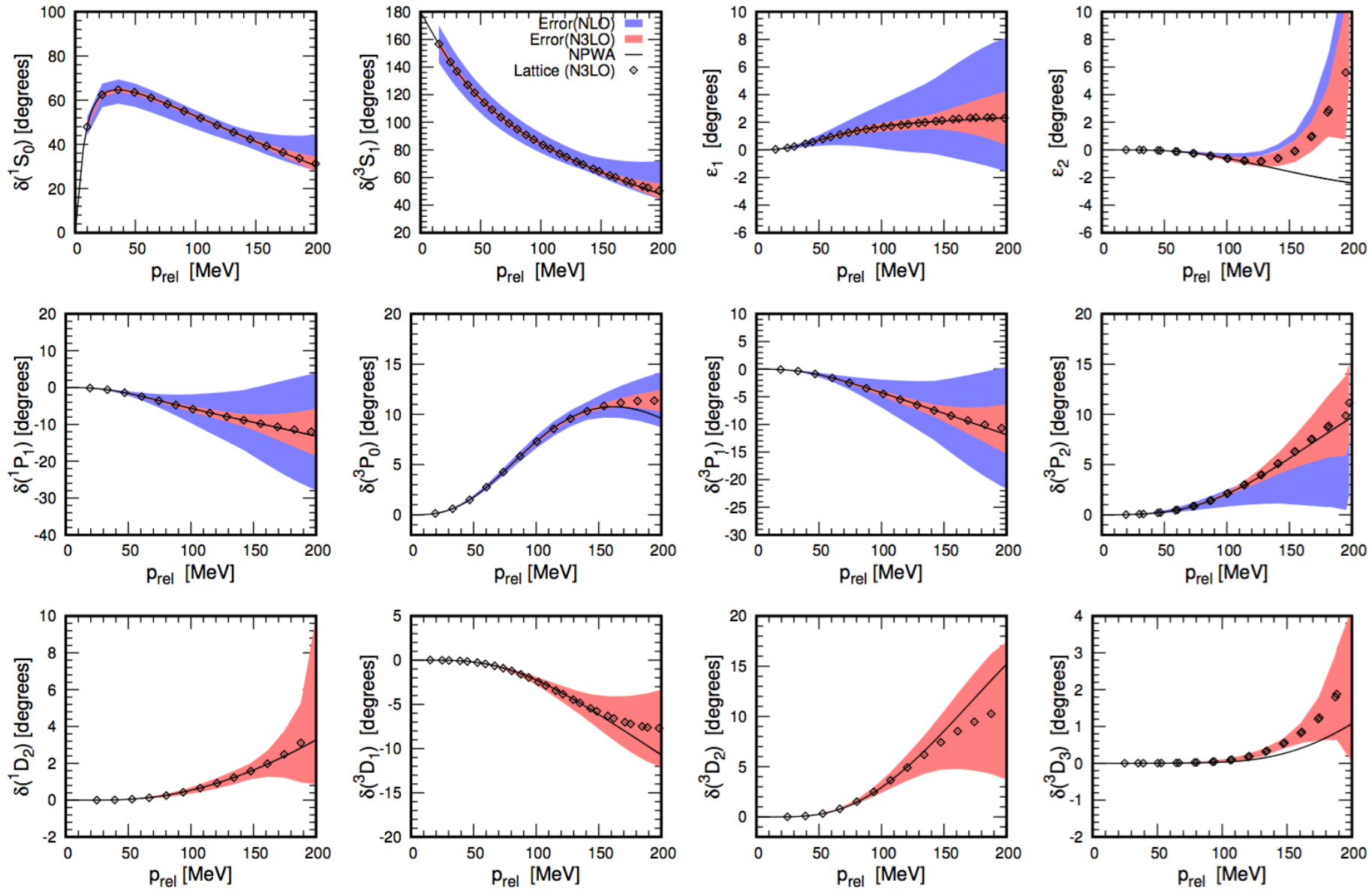
$$\frac{C_0}{2} : \sum_{\mathbf{n}', \mathbf{n}, \mathbf{n}''} \sum_{i', j'} a_{i', j'}^{s_{NL}\dagger}(\mathbf{n}') a_{i', j'}^{s_{NL}}(\mathbf{n}') f_{s_L}(\mathbf{n}' - \mathbf{n}) f_{s_L}(\mathbf{n} - \mathbf{n}'') \sum_{i'', j''} a_{i'', j''}^{s_{NL}\dagger}(\mathbf{n}'') a_{i'', j''}^{s_{NL}}(\mathbf{n}'') :$$

Elhatisari, *et al.*, PRL 119, 222505 (2017); Elhatisari, *et al.*, PRL 117, 132501 (2016)

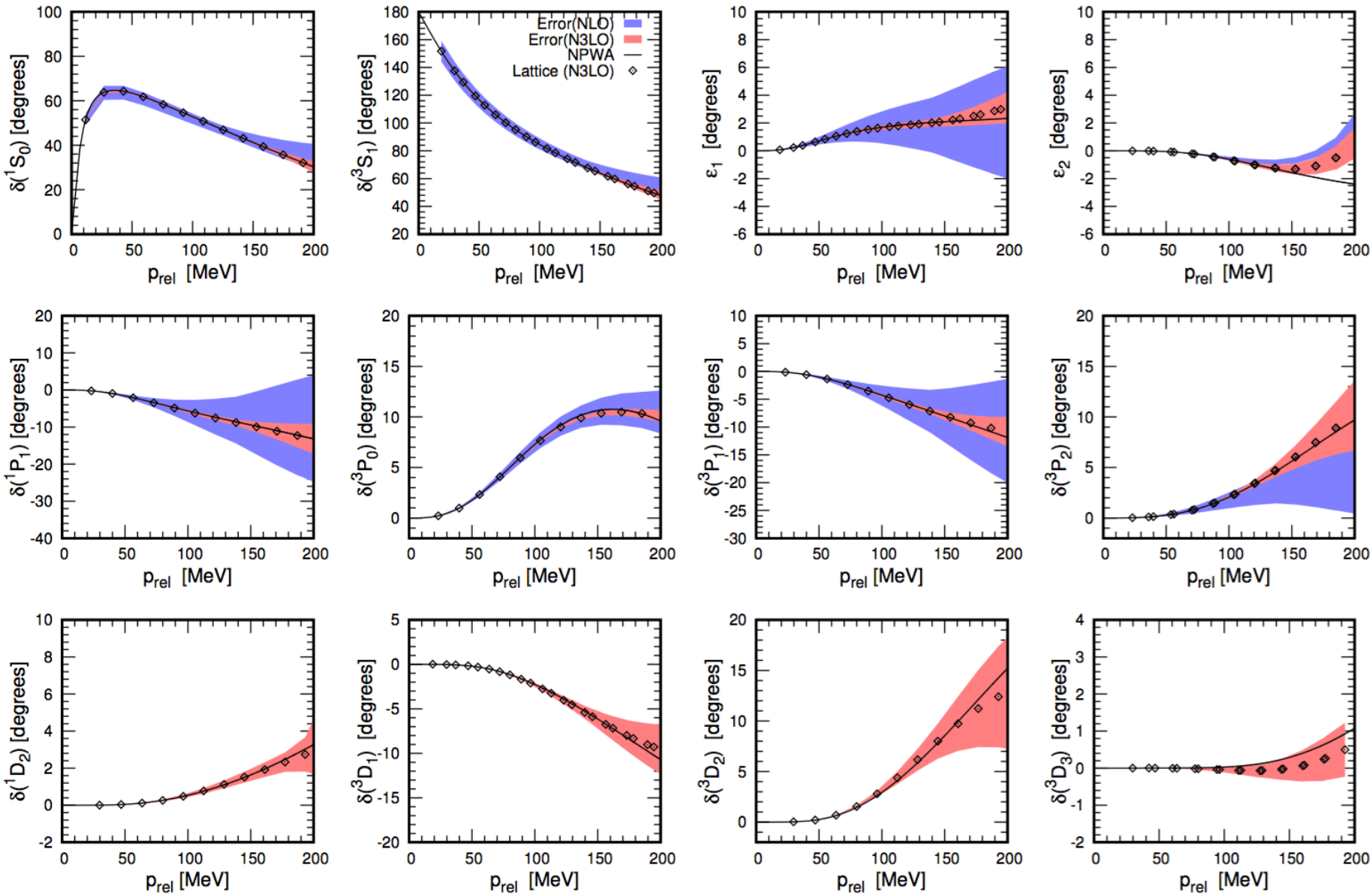
For the long-range interactions, we include the one-pion exchange potential and the two-pion exchange potential for smaller lattice spacings. For coarser lattice spacings, the difference between the two-pion exchange potential and short-range interactions are not resolved. We also include the Coulomb interaction between protons and isospin-breaking interactions.

Li, Elhatisari, Epelbaum, D.L., Lu, Meißner, PRC 98, 044002 (2018)

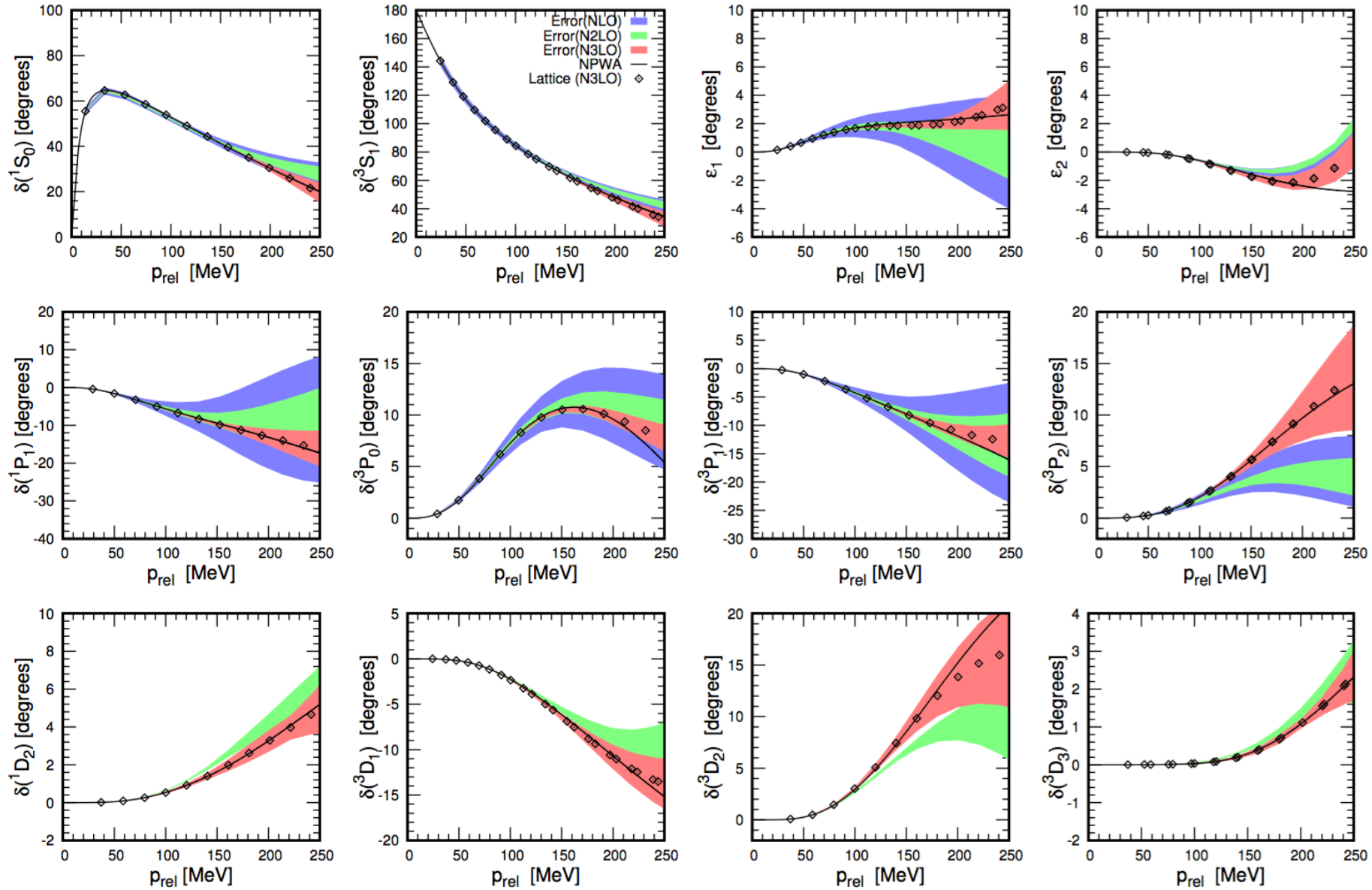
$$a = 1.973 \text{ fm}$$



$$a = 1.644 \text{ fm}$$



$$a = 1.315 \text{ fm}$$



$$a = 0.987 \text{ fm}$$

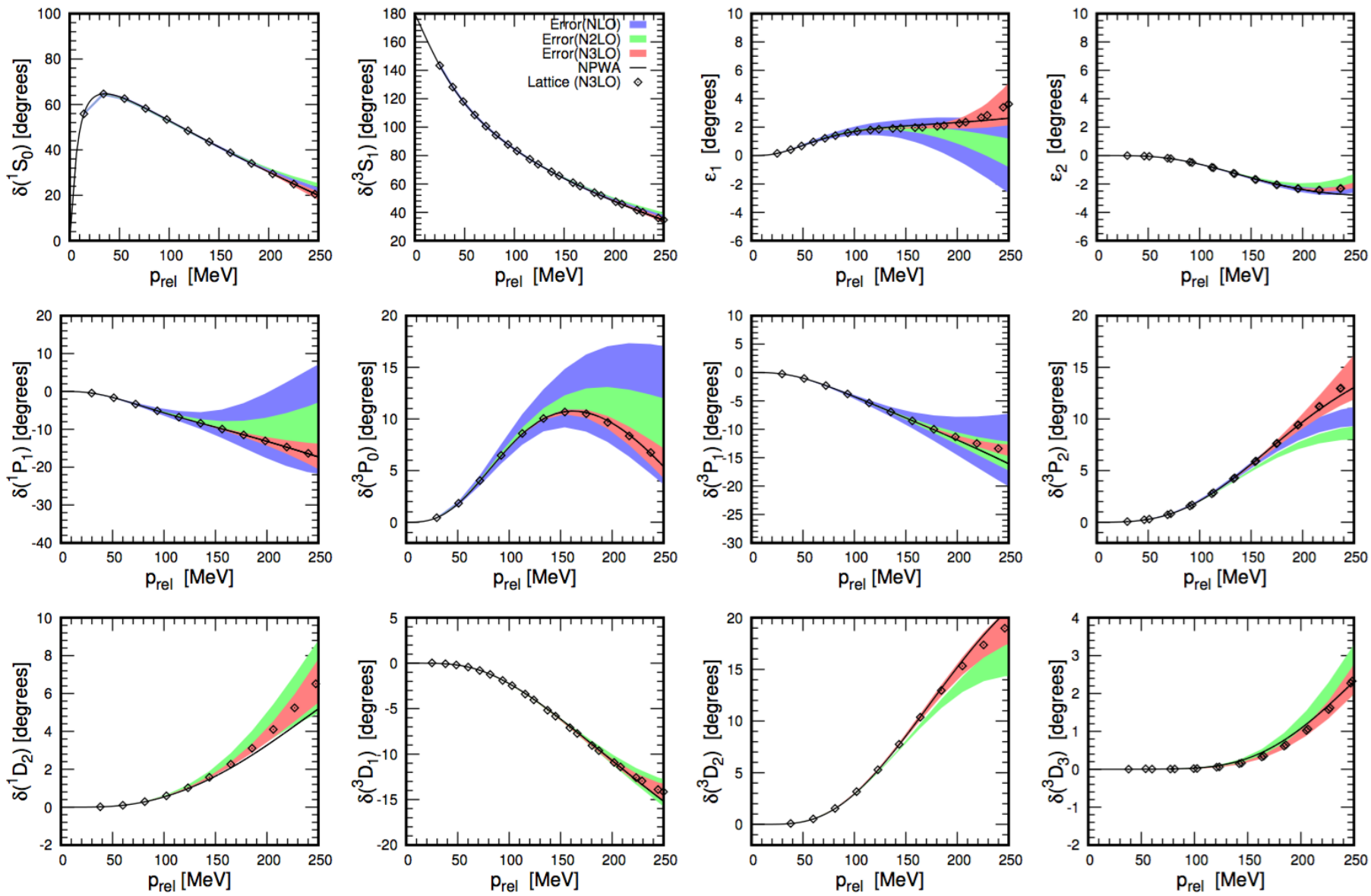


TABLE II. The deuteron properties and S-wave parameters calculated with the full NN interaction up to chiral order $O(Q^4)$ using $a = 0.99$ fm. The error bars we quote in this table indicate uncertainties from the fitting procedure only.

	LO	NLO	N^2 LO	N^3 LO	Empirical
E_d (MeV)	2.2246 ± 0.0002	2.224575 ± 0.000016	2.224575 ± 0.000025	2.224575 ± 0.000011	$2.224575(9)$ [24]
A_s (fm $^{-1/2}$)	0.8662 ± 0.0007	0.8772 ± 0.0003	0.8777 ± 0.0004	0.8785 ± 0.0004	$0.8846(9)$ [25]
η	0.0212 ± 0.0000	0.0258 ± 0.0001	0.0257 ± 0.0002	0.0254 ± 0.0001	$0.0256(4)$ [26]
Q_d (fm 2)	0.2134 ± 0.00000	0.2641 ± 0.0016	0.2623 ± 0.0023	0.2597 ± 0.0013	$0.2859(3)$ [27]
r_d (fm)	1.9660 ± 0.0001	1.9548 ± 0.0005	1.9555 ± 0.0008	1.9545 ± 0.0005	$1.97535(85)$ [28]
a_{3S_1}	5.461 ± 0.000	5.415 ± 0.001	5.421 ± 0.002	5.417 ± 0.001	$5.424(4)$ [29]
r_{3S_1}	1.831 ± 0.0003	1.759 ± 0.002	1.760 ± 0.003	1.758 ± 0.002	$1.759(5)$ [29]
a_{1S_0}	-23.8 ± 0.1	-23.69 ± 0.05	-23.8 ± 0.2	-23.678 ± 0.038	$-23.748(10)$ [29]
r_{1S_0}	2.666 ± 0.001	2.647 ± 0.003	2.69 ± 0.02	2.647 ± 0.004	$2.75(5)$ [29]

Eigenvector continuation

We demonstrate that when a control parameter in the Hamiltonian matrix is varied smoothly, the extremal eigenvectors do not explore the large dimensionality of the linear space. Instead they trace out trajectories with significant displacements in only a small number of linearly-independent directions.

We prove this empirical observation using analytic function theory and the principles of analytic continuation.

Since the eigenvector trajectory is a low-dimensional manifold embedded in a very large space, we can find the desired eigenvector using methods similar to image recognition in machine learning.

D. Frame, R. He, I. Ipsen, Da. Lee, De. Lee, E. Rrapaj, PRL 121 (2018) 032501

Consider a one-parameter family of Hamiltonian matrices of the form

$$H(c) = H_0 + cH_1$$

where H_0 and H_1 are Hermitian. Let the eigenvalues and eigenvectors be

$$H(c)|\psi_j(c)\rangle = E_j(c)|\psi_j(c)\rangle$$

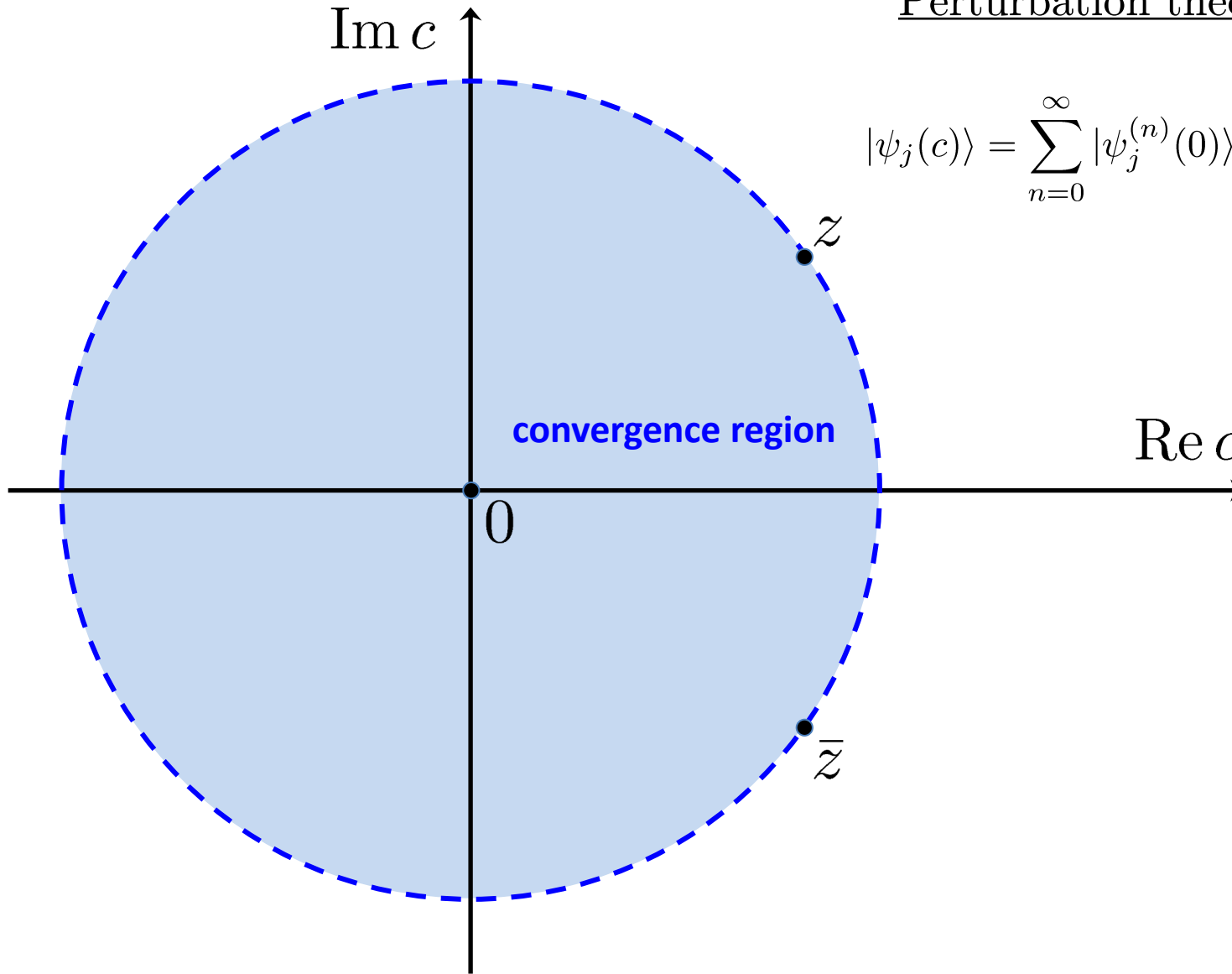
We can perform series expansions around the point $c = 0$.

$$\begin{aligned} E_j(c) &= \sum_{n=0}^{\infty} E_j^{(n)}(0)c^n/n! \\ |\psi_j(c)\rangle &= \sum_{n=0}^{\infty} |\psi_j^{(n)}(0)\rangle c^n/n! \end{aligned}$$

This is the strategy of perturbation theory. We can compute each term in the series when the eigenvalues and eigenvectors of H_0 are known or computable.

Perturbation theory

$$|\psi_j(c)\rangle = \sum_{n=0}^{\infty} |\psi_j^{(n)}(0)\rangle c^n / n!$$



Bose-Hubbard model

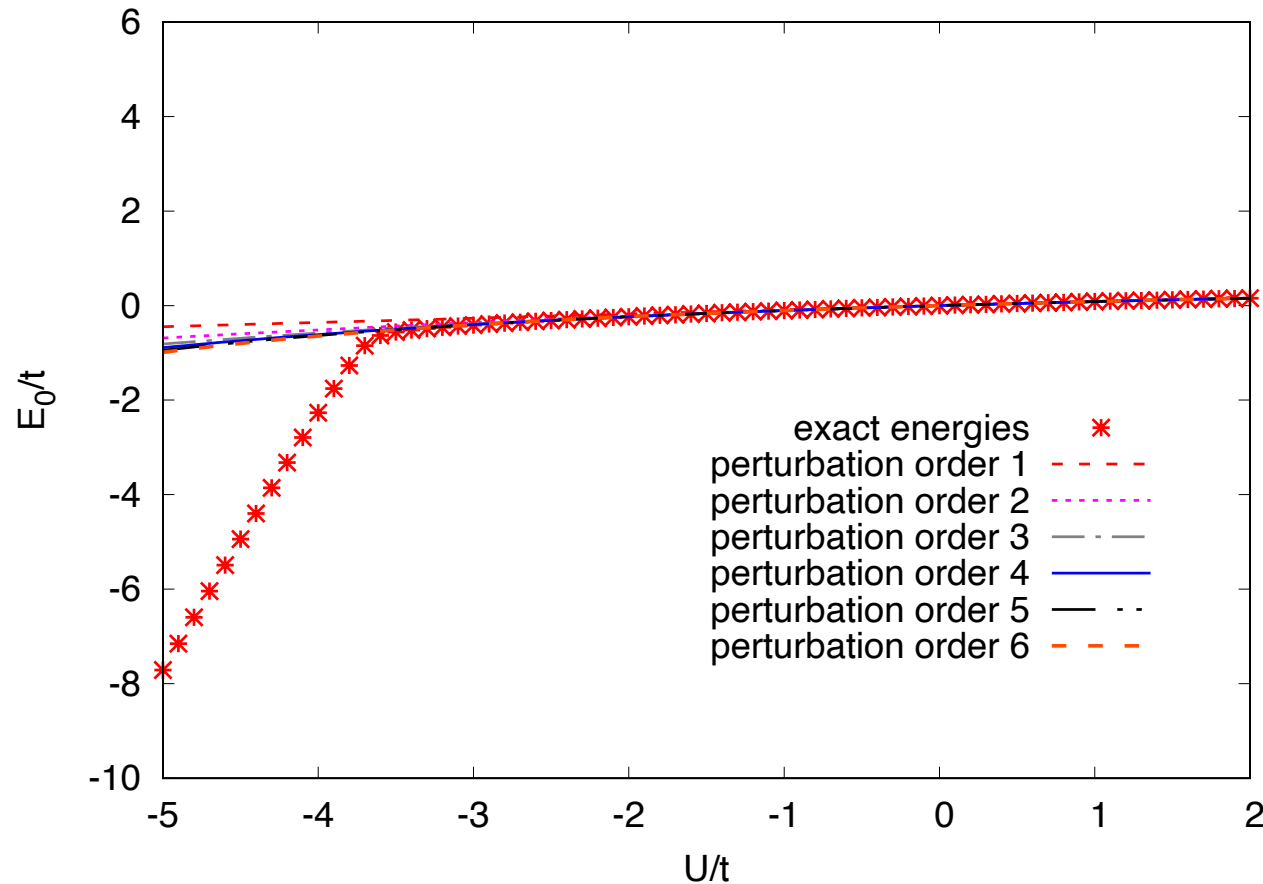
In order to illuminate our discussion with a concrete example, we consider a quantum Hamiltonian known as the Bose-Hubbard model in three dimensions. It describes a system of identical bosons on a three-dimensional cubic lattice.

$$H = -t \sum_{\langle \mathbf{n}', \mathbf{n} \rangle} a^\dagger(\mathbf{n}') a(\mathbf{n}) + \frac{U}{2} \sum_{\mathbf{n}} \rho(\mathbf{n}) [\rho(\mathbf{n}) - 1] - \mu \sum_{\mathbf{n}} \rho(\mathbf{n})$$
$$\rho(\mathbf{n}) = a^\dagger(\mathbf{n}) a(\mathbf{n})$$

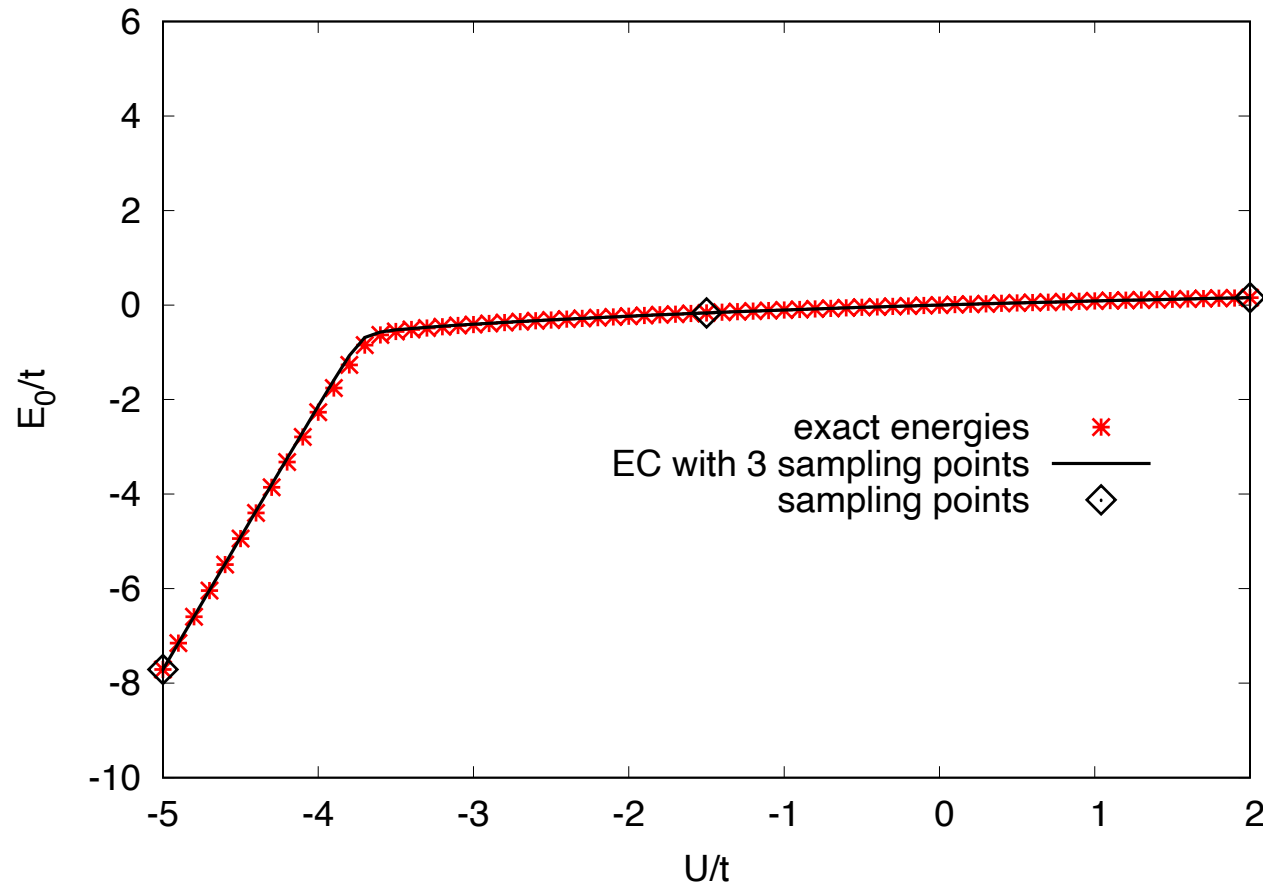
The parameter t controls the hopping the bosons on the lattice, and U is the single-site pairwise interaction. We set the chemical potential to be

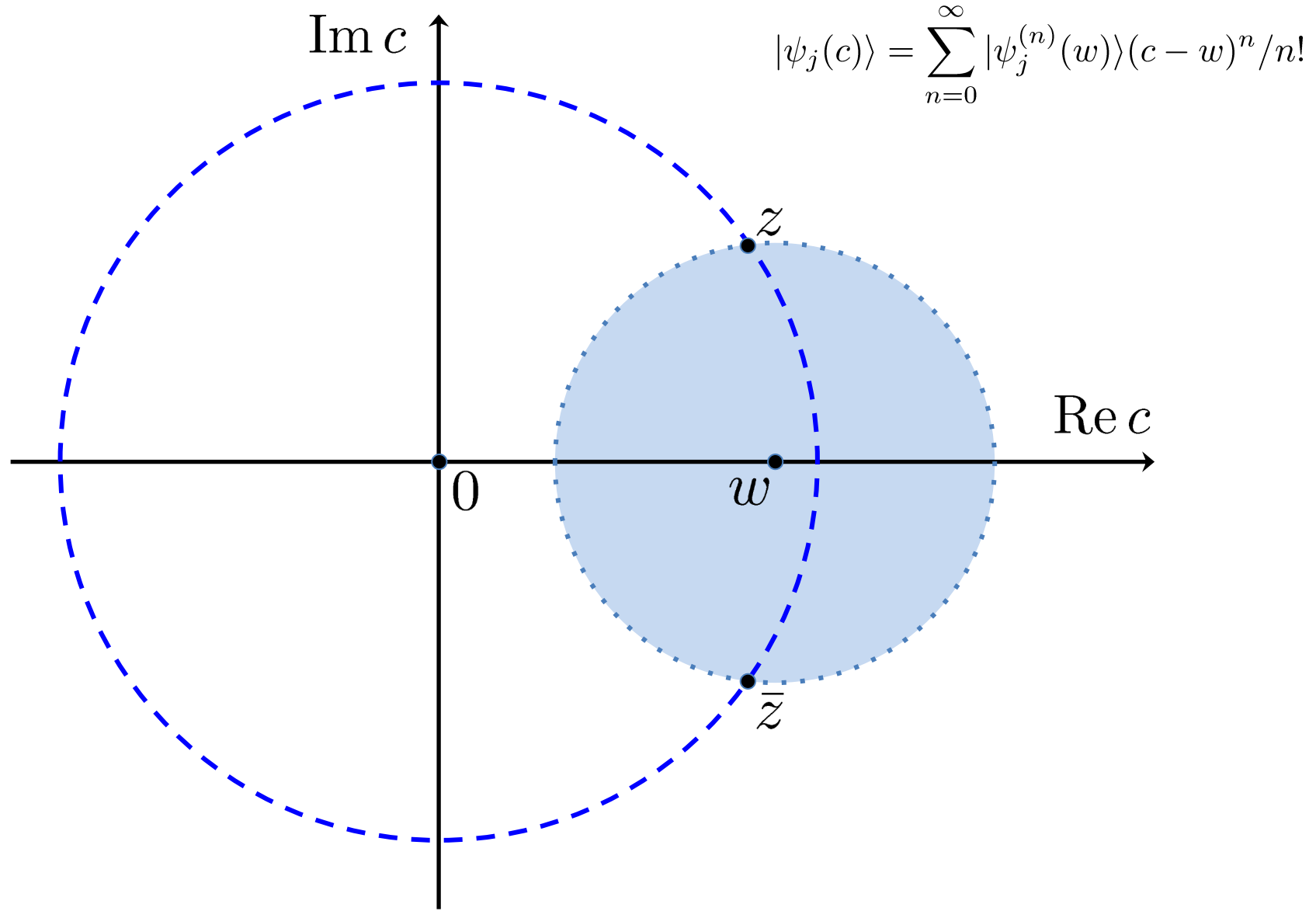
$$\mu = -6t$$

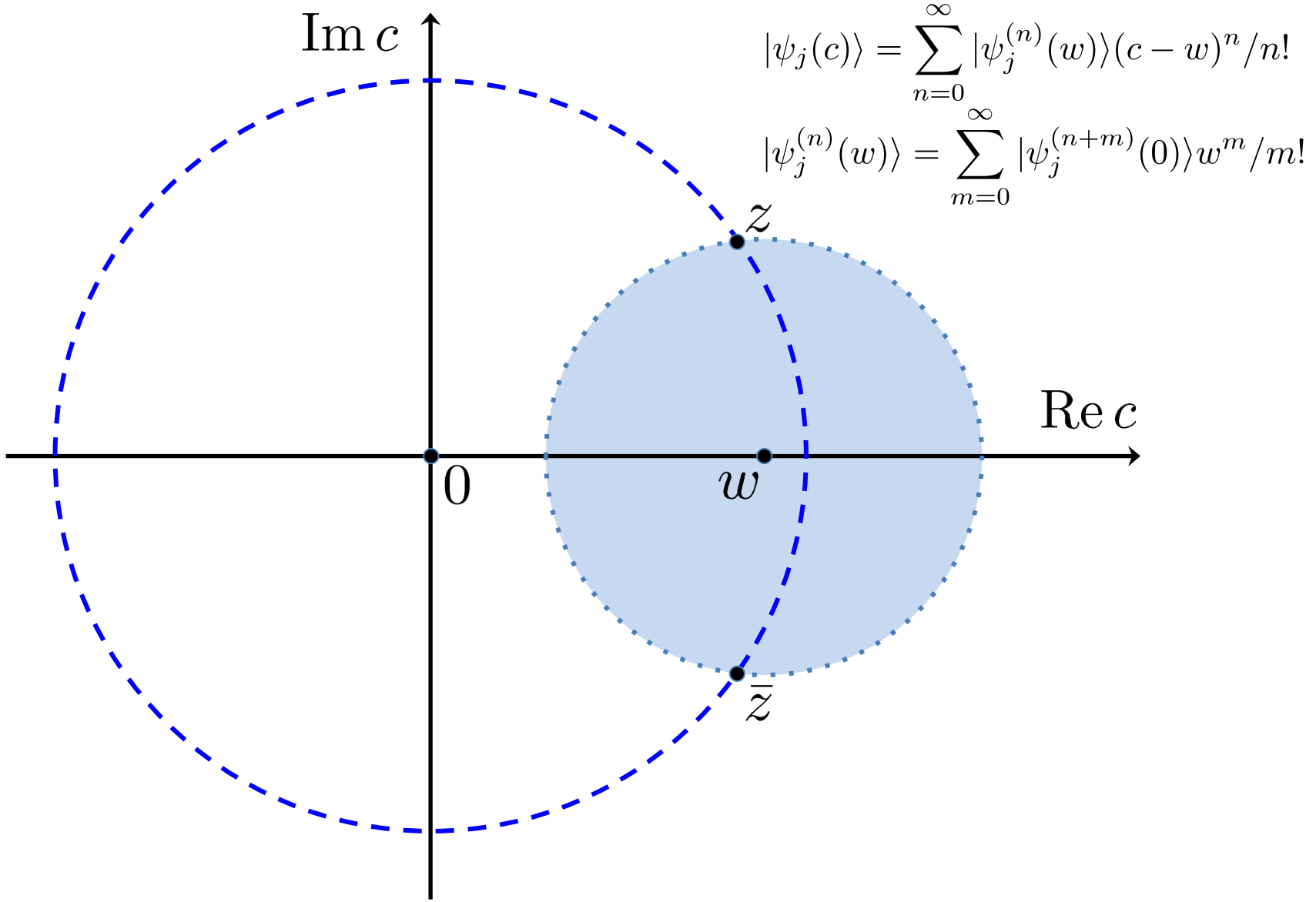
Perturbation theory fails at strong attractive coupling

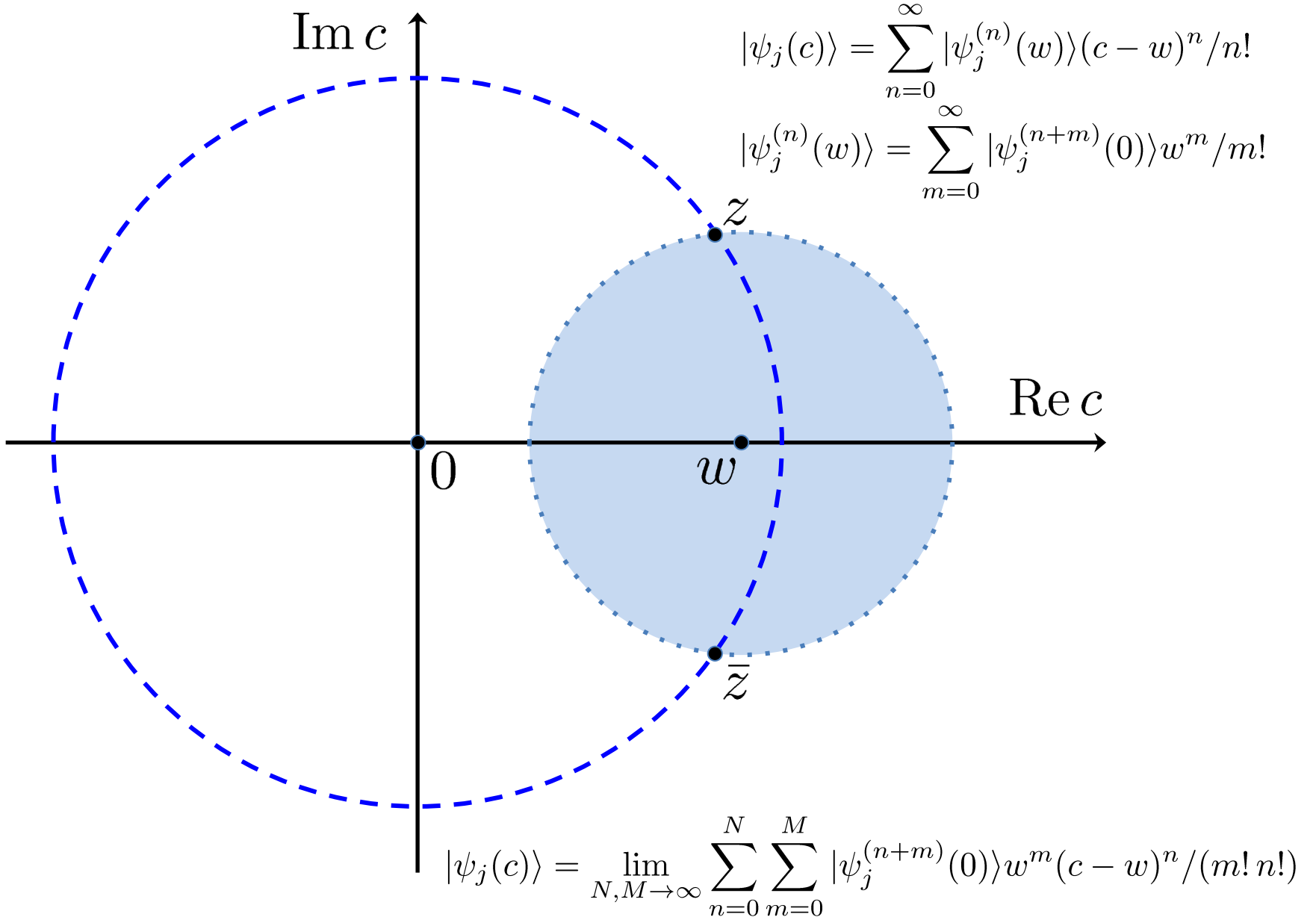


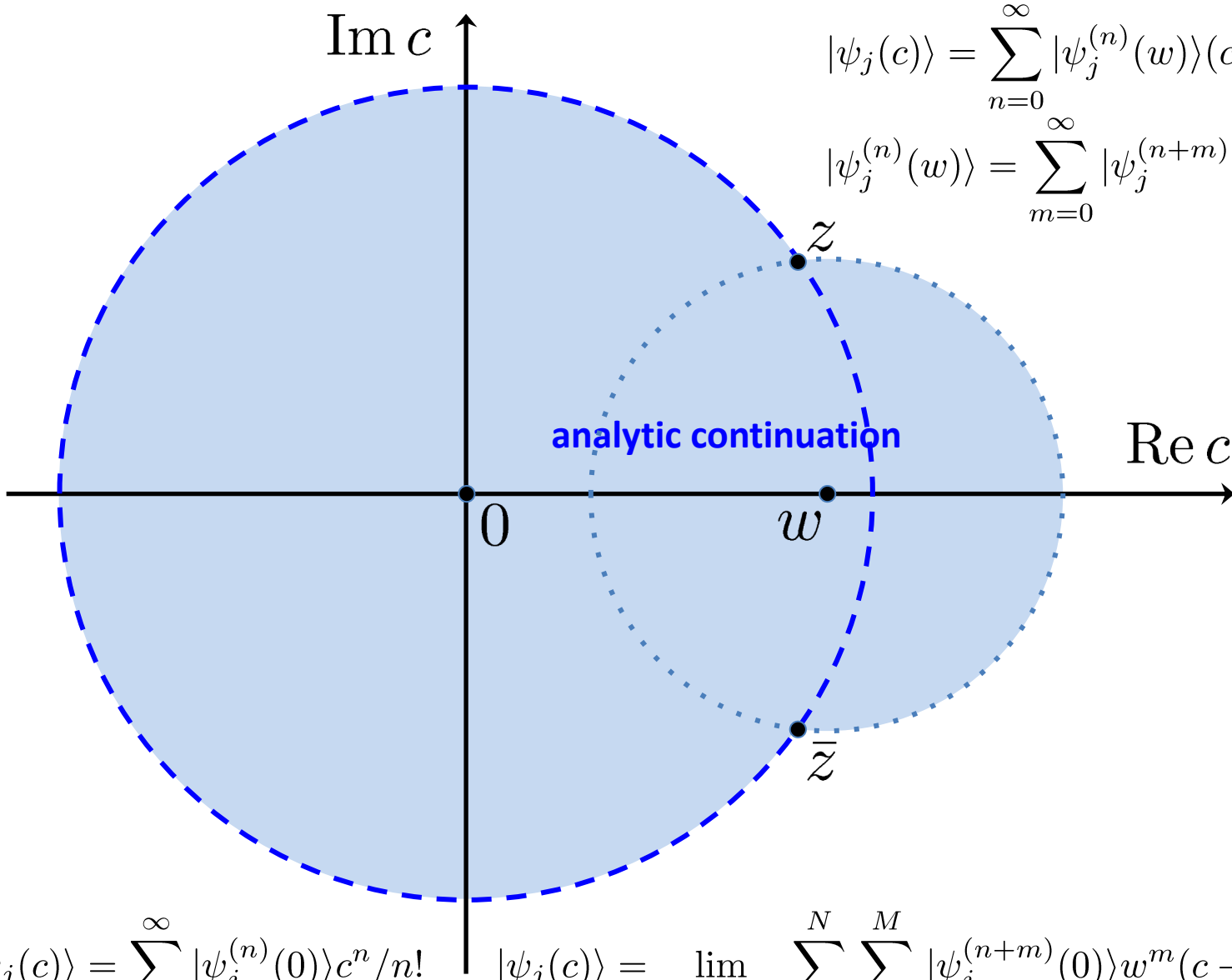
Restrict the linear space to the span of three vectors











$$|\psi_j(c)\rangle = \sum_{n=0}^{\infty} |\psi_j^{(n)}(0)\rangle c^n / n!$$

$$|\psi_j(c)\rangle = \lim_{N,M \rightarrow \infty} \sum_{n=0}^N \sum_{m=0}^M |\psi_j^{(n+m)}(0)\rangle w^m (c-w)^n / (m! n!)$$

The eigenvector can be well approximated as a linear combination of a few vectors, using either the original series expansion

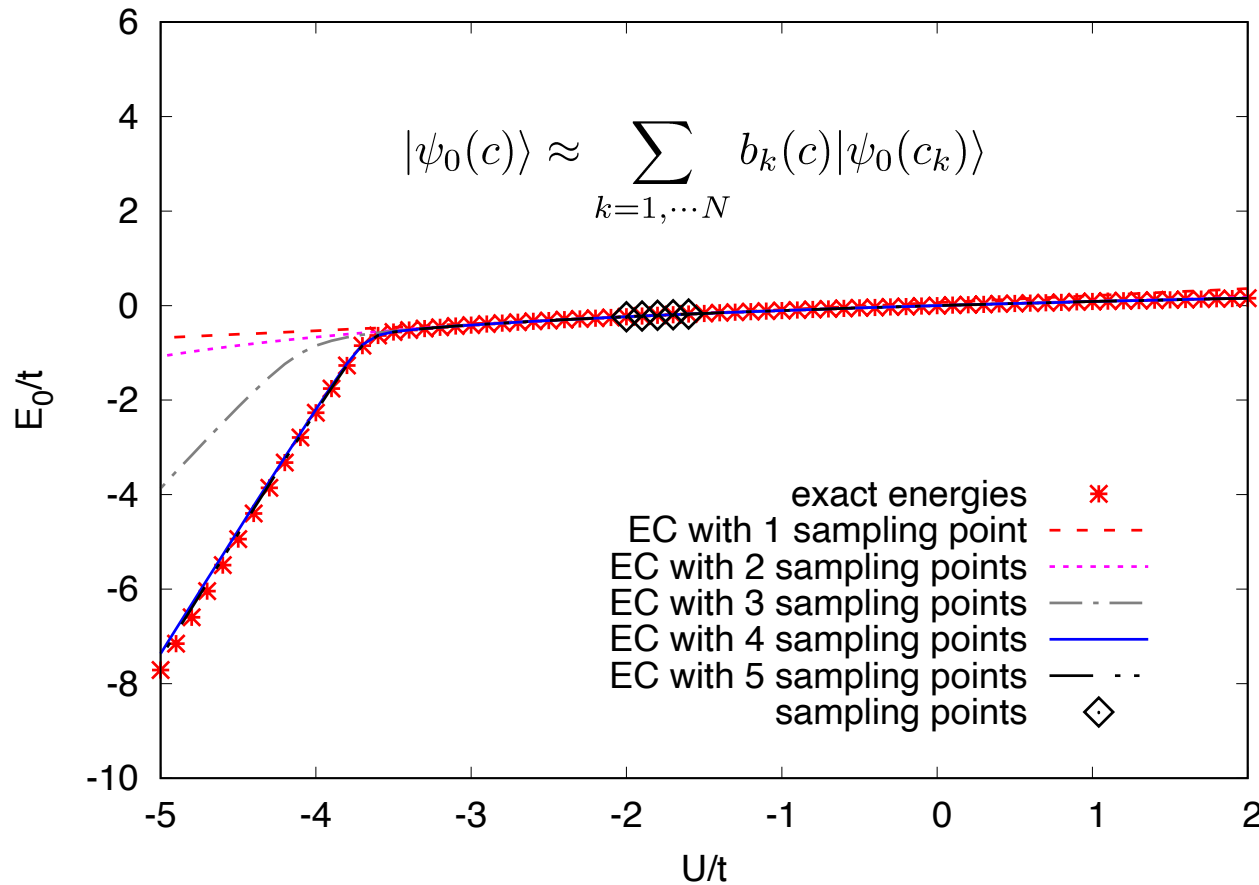
$$|\psi_j(c)\rangle = \sum_{n=0}^{\infty} |\psi_j^{(n)}(0)\rangle c^n / n!$$

or the rearranged multi-series expansion we obtained through analytic continuation

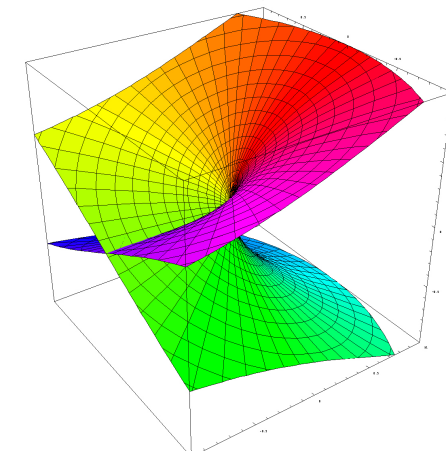
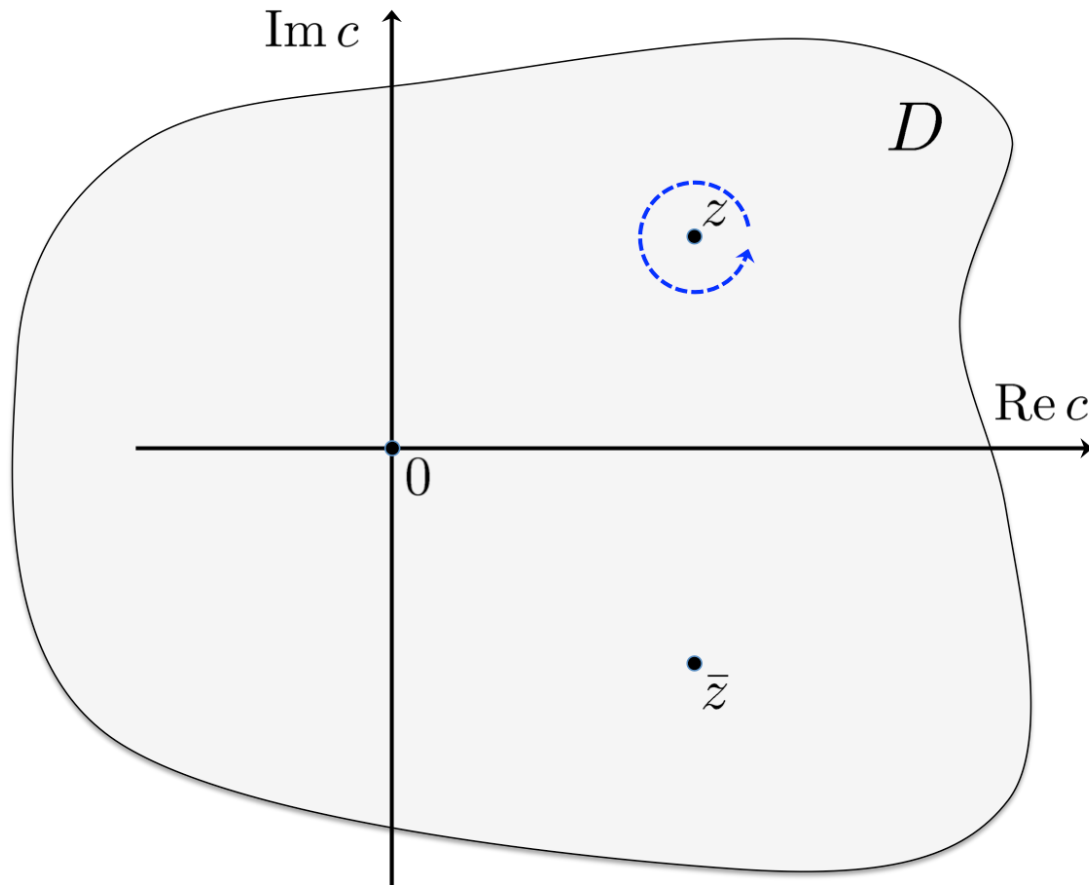
$$|\psi_j(c)\rangle = \lim_{N,M \rightarrow \infty} \sum_{n=0}^N \sum_{m=0}^M |\psi_j^{(n+m)}(0)\rangle w^m (c-w)^n / (m! n!)$$

As c is varied the eigenvector does not explore the large dimensionality of the linear space, but is instead well approximated by a low-dimension manifold.

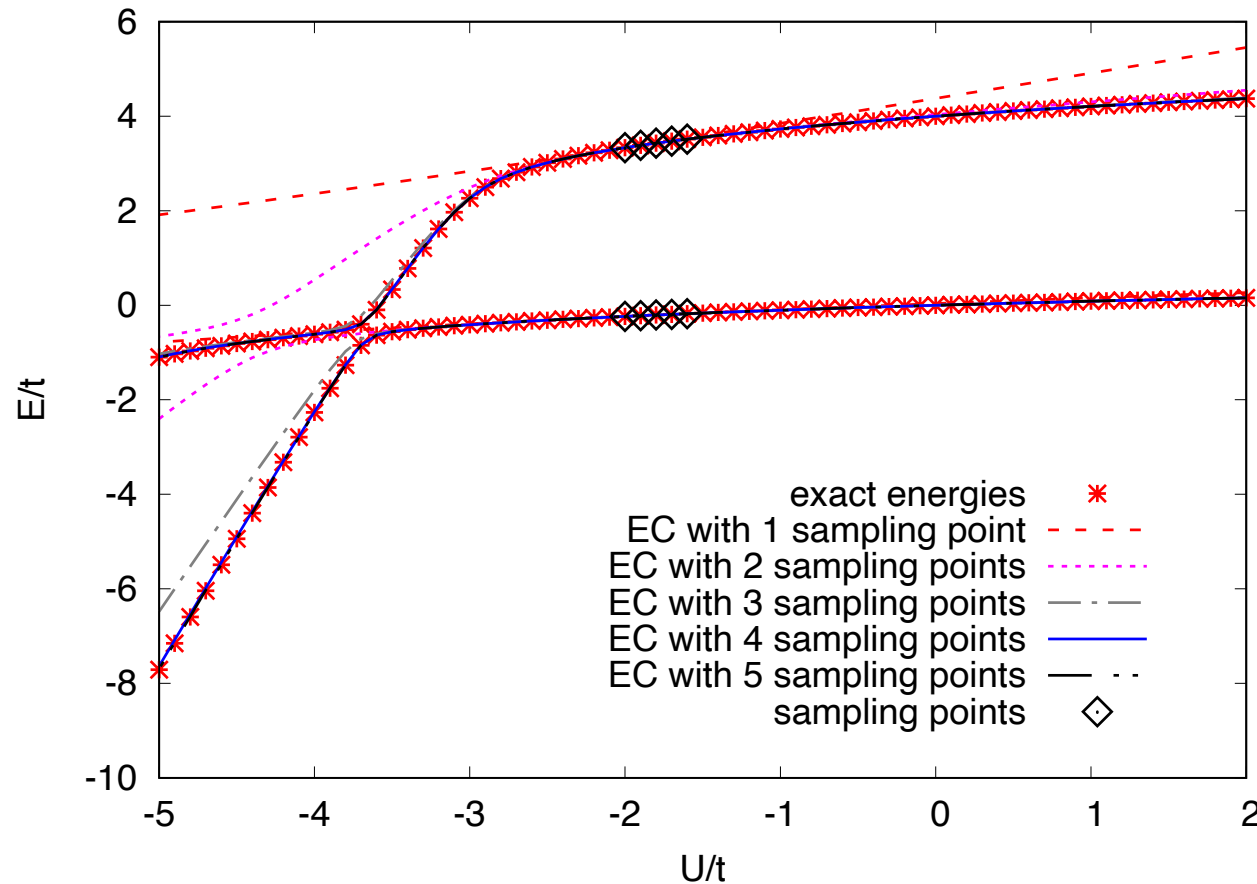
We can “learn” the eigenvector trajectory in one region and perform eigenvector continuation to another region



The Riemann surfaces of the degenerate eigenvectors are entwined at branch point singularities.



Applying eigenvector continuation to more than one eigenvector at a time accelerates convergence near avoided level crossings.



Eigenvector Continuation as an Efficient and Accurate Emulator for Uncertainty Quantification in Nuclear Systems

S. König,^{1, 2,*} A. Ekström,^{3, †} K. Hebeler,^{1, 2, ¶} D. Lee,^{4, §} and A. Schwenk^{1, 2, 5, ¶}

¹*Institut für Kernphysik, Technische Universität Darmstadt, 64289 Darmstadt, Germany*

²*ExtreMe Matter Institute EMMI, GSI Helmholtzzentrum für Schwerionenforschung GmbH, 64291 Darmstadt, Germany*

³*Department of Physics, Chalmers University of Technology, SE-412 96 Göteborg, Sweden*

⁴*Facility for Rare Isotope Beams & Department of Physics and Astronomy, Michigan State University, MI 48824, USA*

⁵*Max-Planck-Institut für Kernphysik, Saupfercheckweg 1, 69117 Heidelberg, Germany*

First principles calculations of atomic nuclei based on microscopic nuclear forces derived from chiral effective field theory (EFT) have blossomed in the past years. A key element of such *ab initio* studies is the understanding and quantification of systematic and statistical errors arising from the omission of higher-order terms in the chiral expansion as well as the model calibration. While there has been significant progress in analyzing theoretical uncertainties for nucleon-nucleon scattering observables, the generalization to multi-nucleon systems has not been feasible yet due to the high computational cost of evaluating observables for a large set of low-energy couplings. In this Letter we show that a new method called eigenvector continuation (EC) can be used for constructing an efficient and accurate emulator for nuclear many-body observables, thereby enabling uncertainty quantification in multi-nucleon systems. On the basis of *ab initio* calculations for the ground-state energy and radius in ${}^4\text{He}$, we demonstrate that EC is more accurate and efficient compared to established methods like Gaussian processes.

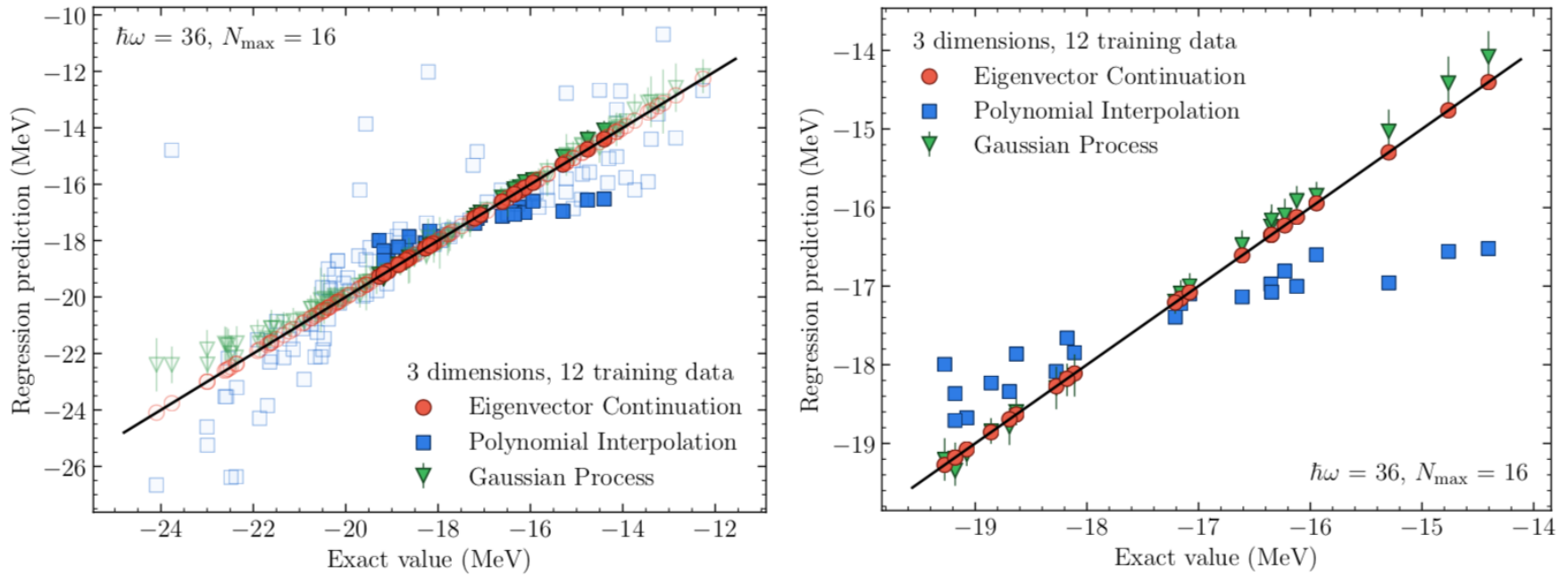


Figure 1. Comparison of different emulators for the ^4He ground-state energy using 12 training data points to explore a space where three LECs are varied. The left panel includes samples for both interpolation (solid symbols) and extrapolation (semi-transparent symbols). See main text on how these are defined. The right panel shows the same data restricted to interpolation samples (note the smaller axis range).

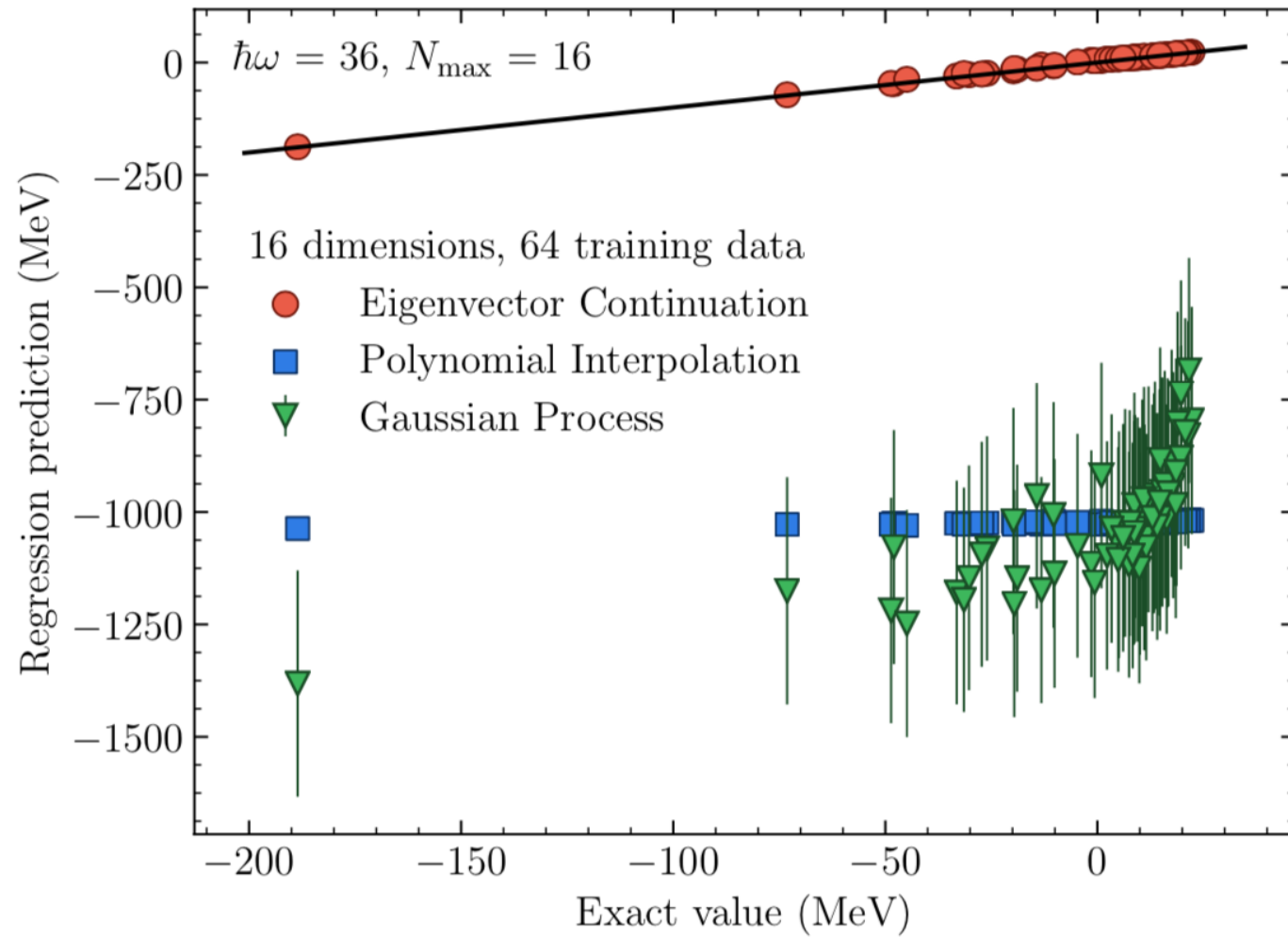


Figure 2. Comparison of different emulators for the ${}^4\text{He}$ ground-state energy using 64 training data points to explore a space where all 16 LECs are varied.

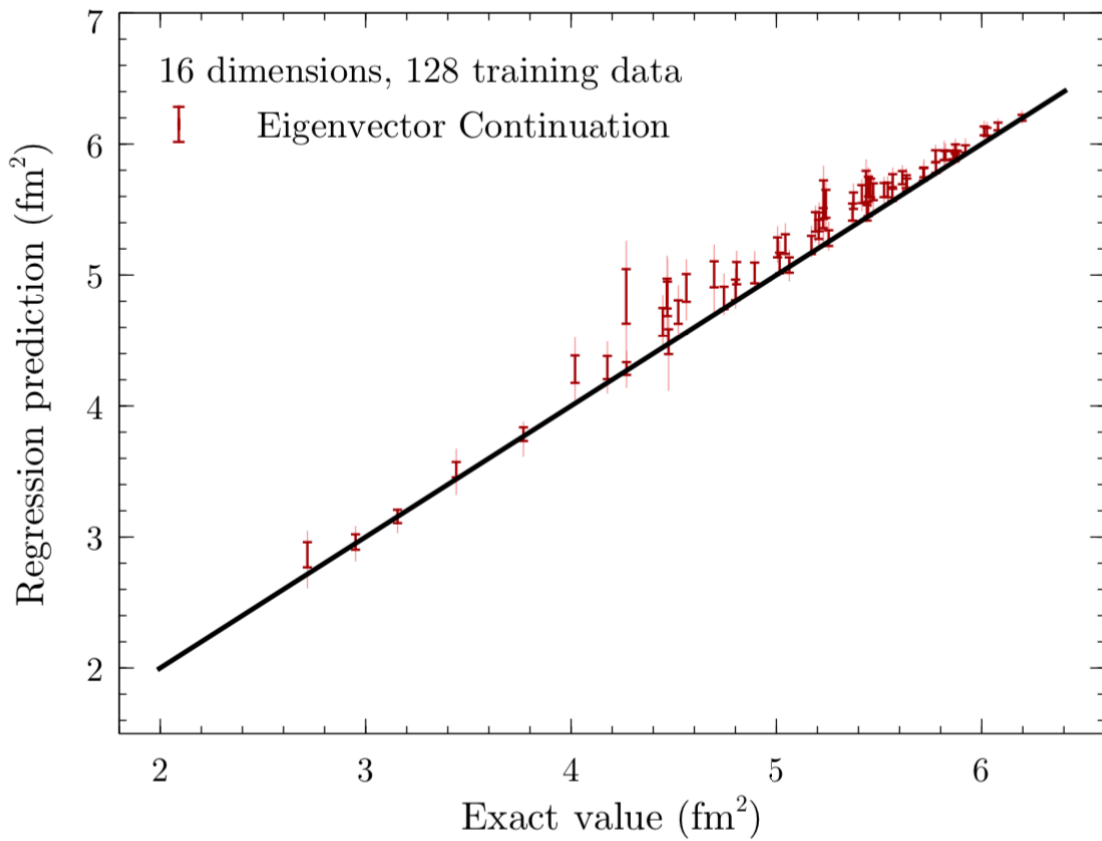


Figure 4. Cross validation for the ${}^4\text{He}$ ground-state radius squared using 128 training data points to explore a space where all 16 LECs are varied. The thicker uncertainty bars indicate 68.2% intervals obtained by considering 32 additional training data sets in addition to the original sample, while the faint thinner ones indicate the full range of results for each point.

Review of topics

Nuclear forces and effective theories

Chiral effective field theory

Spherical wall method

Chiral EFT interactions on the lattice

Eigenvector continuation